IEEE Access
Multidisciplinary | Rapid Review | Open Access Journal

Received May 23, 2019, accepted June 2, 2019, date of publication June 5, 2019, date of current version June 27, 2019.

Digital Object Identifier 10.1109/ACCESS.2019.2921195

Standard Three-Phase Stator Frames for Multiphase Machines of Prime-Phase Order: Optimal Selection of Slot/Pole Combination

AYMAN S. ABDEL-KHALIK[1], (Senior Member, IEEE), AHMED MASSOUD[2], (Senior Member, IEEE), AND SHEHAB AHMED[3], (Senior Member, IEEE)

[1]Department of Electrical Engineering, Alexandria University, Alexandria 21544, Egypt
[2]Department of Electrical Engineering, Qatar University, Doha, Qatar
[3]CEMSE Division, King Abdullah University of Science and Technology, Thuwal 23955, Saudi Arabia

Corresponding author: Shehab Ahmed (e-mail: shehab.ahmed@kaust.edu.sa)

ABSTRACT Multiphase machines have attracted significant attention in both academic and industrial sectors as candidates for high-power safety-critical applications as well as wind energy conversion systems. Undoubtedly, this interest has been fueled by the rapid development in semiconductor devices. Due to the lack of available standard stator frames suitable for constructing multiphase machines of any phase order, machines with multiple three-phase winding sets seem to be the standard topology in many industrial applications. Recent literature has demonstrated a simple generalized technique to rewind a standard three-phase stator frame with a generic prime-phase order stator winding. However, based on the selected slot/pole combination, this technique yields a small unbalance component in the stator phase currents due to the stator leakage inductance mismatch among different phases. This paper further investigates the optimal slot/pole choices, for a given phase-order, that minimize the unbalance in the stator leakage components between phases to ensure comparable performance to standard symmetrical *n*-phase machines. The analysis is presented for the well-known phase orders employed in literature, namely, 5-phase, 7-phase, and 11-phase windings. The effect of winding asymmetry on mathematical modeling and, hence, the dynamic response is also investigated. A 1 kW prototype machine equipped with a five-phase winding is used to experimentally verify the theoretical findings.

INDEX TERMS Multiphase machine, induction motor, three-phase, five-phase, seven-phase, eleven-phase, star of slots, leakage inductance calculation, multilayer winding.

NOMENCLATURE

i	Current
v	Voltage
λ	Flux linkage
R	Winding resistance
G	Conductance
L	Self or magnetizing inductances
l	Leakage inductance
p	Number of pole pairs
n	Number of stator phases
N_{ph}	Number of turns per stator phase
N_c	Number of conductors per slot for the original three-phase stator.
T_e	Developed torque
ω_r	Electrical rotor angular speed

Subscripts

$\alpha\beta$	Fundamental subspace components
xy	Secondary subspace components
s	Stator
r	Rotor
m	Mutual/Magnetizing
t	Top
b	Bottom

The associate editor coordinating the review of this manuscript and approving it for publication was Xiaodong Sun.

I. INTRODUCTION

The past decade has witnessed extensive academic interest in multiphase machines and drive systems for different industrial applications [1]. The interest in these high phase order

systems arguably represents a promising opportunity to meet the stringent standards of certain safety-critical applications [1]–[8]. The selection of an optimum number of phases remains a questionable choice that not only entails several cost/complexity tradeoffs but also is, in fact, an application-dependent parameter [1]. Although the employment of multiphase machines in industrial applications may have started a few decades ago, the six-phase machines have since solely been prevailing in most applications [9]–[11]. That was mainly dictated by different practical and technological constraints at this early stage of development. Early key papers in multiphase machines actually did not recommend the use of a prime number of phases due to these constraints [12]. More recent literature, however, demonstrated that machines with a prime number of phases, including five- [4], [13], seven- [14], [15], or eleven-phase [16], potentially offer numerous attractive merits over machines with multiple three-phase windings. This includes better torque density through harmonic injection without additional hardware components [16], [17], the feasibility to employ single layer windings while preserving a high quality of flux distribution [18], and the relatively better fault-tolerant capability [19].

Nevertheless, it is fair to acknowledge that industry is still reluctant to adopt this technology, and machines with multiple three-phase winding sets seem to be the favored option in many industrial sectors since the well-established three-phase technology and, therefore, the readily off-the-shelf three-phase converters can still be utilized. Additionally, stators with multiple three-phase winding sets can, in most cases, be constructed using standard three-phase stator frames without many constraints. As a matter of fact, all available stator frames provided by most electric motor manufacturers are still limited to standard three-phase designs. Therefore, building a stator frame with a number of slots different from these standard frames will certainly be a higher cost custom task, especially for high power designs.

The work done in [20] introduced a simple and generalized technique to construct a prime-phase order multiphase winding using standard three-phase stator frames. The presented winding layout was based on the Star of Slots (SoS) theory [21] combined with the concept of stator winding shifting [22] to design the number of turns of the series-connected coils belonging to each phase that not only ensures a zero backward MMF component, but also results in a high-quality flux distribution. Additionally, the total number of turns per phase is the same for all phases to ensure equal stator resistance for all phases. The proposed layout in [20] was introduced for the five-, seven-, and eleven-phase orders. By taking an existing three-phase stator frame as a benchmark, a better flux distribution at a higher fundamental flux component was achieved for the same copper volume with these proposed winding layouts. Interestingly, the given layouts can also enhance the machine torque density for a certain core volume; the gain in the fundamental torque producing flux component increases with the adopted phase order. The concept of harmonic injection was also proven to be applicable since machine torque/current gain was comparable to conventional symmetrical n-phase windings of the same phase-order.

On the other hand, this winding layout resembles a more complicated stator structure than standard winding layouts. Being structurally based on series-connected coils with a different number of turns, this winding layout was shown to yield a small secondary sequence current component due to the difference in the leakage stator inductances of different phases. Therefore, it was concluded in [20] that the presented solution represents a compromise, rather than an optimum solution to make use of the available stator frames in constructing prime-phase order multiphase machines. Moreover, the solution was presented as a means to bridge the gap in multiphase drive systems research, since it enables interested researchers to access the required technology platform with minimal barriers.

This papers further investigates the concept presented in [20] with an additional major objective to derive a mathematically-verified optimal selection criterion to choose a suitable standard stator frame for a given number of phases. This criterion aims to minimize the effect of the induced secondary current component experienced due to the unavoidable mismatch in the stator leakage inductance of different phases. It will also be mathematically proven that the effect of the small mismatch between the stator leakage inductance of different phases has a minimal/no effect on the machine dynamic performance. The traditional vector space decomposition (VSD) for a symmetrical n-phase winding is proved to successfully decompose the phase variables of this winding layout into decoupled subspaces with small cross-coupling terms depending on the adopted slot/pole combination. A mathematical model to represent this leakage inductance mismatch is also presented.

II. PRIME-PHASE ORDER MULTIPHASE WINDING USING STANDARD THREE-PHASE FRAMES

In [20], the design steps to rewind a standard three-phase stator frame with any n-phase winding having a prime-phase order are detailed. The concept is simply based on the SoS theory by first assuming a single layer winding, where each phase comprises a number of series-connected coils with a different number of turns, in general, based on the available number of slots. The SoS theory [21] is used to calculate the required number of turns for each coil such that balanced n-phase emf voltages are obtained across all phases. To achieve such a goal, this initial single-layer design will mostly experience a notable diversion between the number of conductors per slot in different stator slots. The stator shifting concept [22] is, therefore, used to minimize this diversion by employing a multilayer winding design. For the sake of winding simplicity, the design criterion given in [20] was constrained to double-layer layouts.

The concept given in [20] was given for the most common number of slots/pole, namely 6, 9, 12, 18 and for a number of phases of 5, 7, and 11. It has been concluded based on

Phase (j)		a	b	c	d	e				
Slot (i)		1	2	3	4	5	6	7	8	9
$\frac{N_{ij}}{N_c}$	U	a (0.9)	-d (0.2)	-d (1)	b (0.35	b (1.1)	-e (0.55)	-e (1.1)	c (0.8)	- a (0.1)
	L	- c (0.2)	a (0.9)	a (0.1)	-d (0.8)		b (0.55)		-e (0.35)	c (1)

U: upper layer, L: Lower layer, and N_{ij}: number of turns of coil i of phase j

FIGURE 1. 18-slot/2-pole five-phase winding layout.

Phase (j)		a	b	c	d	e	f	g		
Slot		1	2	3	4	5	6	7	8	9
$\frac{N_{ij}}{N_c}$	U	a (0.86)	-e (0.72)	b (0.44)	-f (0.15)	-f (0.86)	c (0.86)	-g (0.58)	d (0.29)	-a (0.08)
	L		a (0.08)	-e (0.29)	b (0.58)			c (0.15)	-g (0.44)	d (0.72)

FIGURE 2. 18-slot/2-pole seven-phase winding layout.

Phase (j)		a	b	c	d	e	f	g					
Slot		1	2	3	4	5	6	7	8	9	10	11	12
$\frac{N_{ij}}{N_c}$	U	a (0.72)	-e (0.22)	-e (0.78)	b (0.45)	b (0.78)	-f (0.66)	c (0.12)	c (0.78)	-g (0.33)	-g (0.78)	d (0.56)	-a (0.06)
	L	-d (0.22)	a (0.72)	a (0.06)	-e (0.56)		b (0.33)	-f (0.78)	-f (0.12)	c (0.66)		-g (0.45)	d (0.78)

FIGURE 3. 24slot/2-pole seven-phase winding layout.

Phase (j)		a	b	c	d	e	f	g	h	i	j	K	
Slot		1	2	3	4	5	6	7	8	9	10	11	12
$\frac{N_{ij}}{N_c}$	U	a (0.91)	-g (0.91)	b (0.82)	-h (0.73)	c (0.64)	-i (0.55)	d (0.46)	-j (0.37)	e (0.28)	-k (0.19)	f (0.1)	-a (0.05)
	L		a (0.05)	-g (0.1)	b (0.19)	-h (0.28)	c (0.37)	-i (0.46)	d (0.55)	-j (0.64)	e (0.73)	-k (0.82)	f (0.91)

FIGURE 4. 24slot/2-pole eleven-phase winding layout.

Finite Element Analysis (FEA) that the best choice seems to be the one which corresponds to a number of slots close to or higher than the number of slots of a standard n-phase winding. For example, the standard five-phase stator commonly entails 20 slots/pole-pair (with a number of slots/phase/pole $q = 2$). An 18-slot stator was shown effective to obtain a balanced five-phase winding. Similarly, a standard 2-pole seven-phase winding entails 28 slots ($q = 2$); the closest standard three-phase frame will have 24 slots. An 18-slot stator, however, yields a notable secondary sequence current component, as explained in [20]. Finally, a 22-slot stator with a concentrated winding can be used to construct an eleven-phase stator with a high-quality flux distribution; the closest standard three-phase frame will have 24 slots.

Table 1 summarizes the feasible slot/pole values for a different number of phases which yield winding layouts with only two layers while providing high-quality flux distributions and acceptable slot filling factors [20]. Figs. 1-4 show the winding layouts for some important cases, upon which the given analysis in this paper will then be based.

TABLE 1. Possible n-phase winding layouts for different slot/pole combinations.

Phase / S/pole	Five	Seven	Eleven
6	Valid	Invalid	Invalid
9	Valid	Valid	Invalid
12	Valid	Valid	Valid
18	Valid	Valid	Complex

Invalid option
Valid
Valid with notable stator current unbalance
Valid but complex winding - higher than two layers

III. COMPARISON WITH STANDARD SYMMETRICAL N-PHASE WINDING

Although the concept presented in [20] generally yields winding layouts having an equal total number of turns and equal stator resistance for all phases, the difference in the number of turns for separate coils comprising each phase will cause a certain degree of asymmetry in the stator impedance of different phases. This is due to the difference in the stator leakage inductance components between the different phases. Hence, in order to verify that these winding layouts can successfully emulate/approximate standard symmetrical n-phase windings, the following points should be mathematically verified:

1. The magnetizing component, and hence the magnetizing inductance, of all phases should be the same for all sequences.
2. The self and mutual components of the stator leakage inductance of different phases should be very close in order to minimize the impedance mismatch between phases.
3. The employment of standard VSD transformation for symmetrical n-phase windings given by (1) to decompose the phase variables of the proposed winding layouts will eventually yield decoupled subspaces.

These points are mathematically investigated in the following subsections based on a comparative study with equivalent standard n-phase windings.

$$[T]=\frac{2}{n}\times\begin{bmatrix}1 & \cos\alpha & \cos 2\alpha & \dots & \cos(n-1)\alpha\\ 0 & \sin\alpha & \sin 2\alpha & \dots & \sin(n-1)\alpha\\ 1 & \cos 3\alpha & \cos 6\alpha & \dots & \cos 3(n-1)\alpha\\ 0 & \sin 3\alpha & \sin 6\alpha & \dots & \sin\ 3(n-1)\alpha\\ \vdots & \vdots & \vdots & \vdots & \vdots\\ 1 & \cos(n-2)\alpha & \dots & \dots & \dots\\ 0 & \sin(n-2)\alpha & \dots & \dots & \dots\\ \frac{1}{2} & \frac{1}{2} & \frac{1}{2} & \dots & \frac{1}{2}\end{bmatrix} \quad (1)$$

where $\boldsymbol{\alpha = 2\pi/n}$

A. SEQUENCE COMPONENTS OF MAGNETIZING FLUX

It is required in this proof to verify that the winding layouts given in [20] will provide comparable magnetizing flux distribution, and, consequently, sequence flux components, as the standard n-phase winding. This is carried out by investigating the harmonic flux mapping among available subspaces for different phase orders represented by the following cases assuming 2-pole winding layouts:

1. *Conventional five-phase* winding using 20-slot stator.
2. *Proposed five-phase* winding using 18-slot stator.
3. *Conventional seven-phase* stator using 28-slot stator.
4. *Proposed seven-phase* winding using 18-slot stator.
5. *Proposed seven-phase* winding using 24-slot stator.
6. *Conventional eleven-phase* stator using 22-slot stator.
7. *Proposed eleven-phase* winding using 24-slot stator.

The conventional n-phase cases for the 5, 7, and 11-phase stators are used for benchmarking. A standard 1Hp, 4-pole, 400V, 50Hz, 36-slot standard three-phase machine is used for this comparative study and for experimental verification. The machine rated speed and current are 1320 rpm and 2.1A, respectively. For the same rotor, the required stator designs to accommodate the previous n-phase winding examples are calculated, while the same total number of active conductors is assumed equal for all designs to ensure the same machine total power [23]. The original three-phase machine has a number of conductors per slot equal to 84 conductors with a conductor diameter of 0.56 mm. The total number of turns per phase will be 252 turns. Correspondingly, and for the same rated phase current, the total number of turns per phase will, therefore, be 150, 108, and 69 turns for the five-, seven, and eleven-phase windings, respectively. As explained in [23], the new phase voltages for these equivalent machines that ensure the same total power will be $(3/5)\times 230V = 138V$, $(3/7)\times 230V = 98.6V$, and $(3/11)\times 230V = 62.7V$ for the five-, seven-, and eleven-phase stators, respectively.

Based on these cases, the MMF distributions of different phases are obtained from their corresponding turn functions at a certain time instant assuming a unit stator current magnitude. The sequence components are then determined from the phase MMF distributions by applying the VSD transformation given by (1). The harmonic spectra of different sequence components are then found for the different cases. FEA is also used to support the theoretical findings.

1) FIVE-PHASE CASE

The winding shown in Fig. 1 is compared with a standard 20-slot single-layer symmetrical five-phase stator winding with $q = 2$ and the same total number of turns per phase. For this phase order, there are two main subspaces and one zero-sequence component. Under star connection, the effect of the zero-sequence component is discarded. The harmonics with order $10k \pm 1$ are mapped to the fundamental $\alpha\beta$ subspace, while those with order $10k \pm 3$ are mapped to the xy secondary subspace. Based on (1), the MMF sequence components are shown in Fig. 5. Clearly, the harmonic mapping for the proposed and the conventional five-phase winding layouts can be assumed identical, which proves that a complete decoupling, in terms of the magnetizing (torque producing) flux components, can be a fair assumption.

2) SEVEN-PHASE CASE

For this phase order, there are two secondary subspaces, namely, xy_1 and xy_2. The seven-phase winding layouts shown in Figs. 2 and 3 for the 18-slot/pole-pair and the 24-slot/pole-pair stators, respectively, are compared with a standard 28-slot seven-phase single-layer winding layout with $q = 2$. It has been mentioned before that the closer the number of slots to the conventional n-phase case is, the better the MMF distribution is expected to be. The MMF sequence

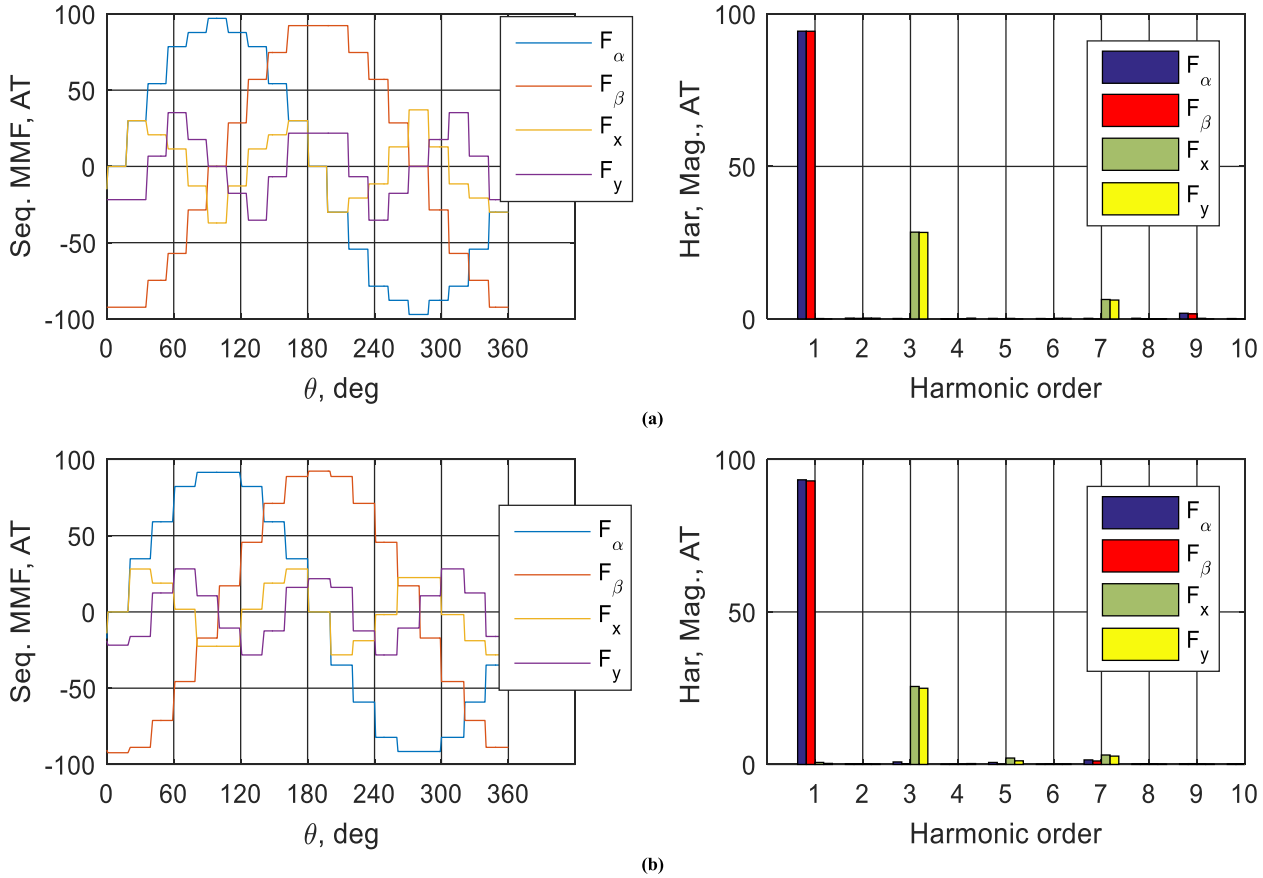

FIGURE 5. MMF sequence components for the five-phase case (a) Conventional five-phase stator using 20-slot stator. (b) Proposed five-phase winding using 18-slot stator.

components of a conventional 7-phase case using a 28-slot/pole pair are given in Fig. 6(a). By investigating the MMF sequence components of the 18-slot and 24-slot stators shown in Figs. 6(b) and (c), respectively, the latter winding corresponds to a better flux distribution; it highly approximates the standard 28-slot seven-phase stator. On the other hand, the MMF $\alpha\beta$ components of the 18-slot/pole-pair stator are slightly unbalanced, and small coupling between different subspaces will likely take place. This will expectedly yield a notable unbalance in the phase currents. To support this conclusion, FEA is used to simulate the phase currents under rated operation of the 18-slot/pole-pair and 24-slot/pole-pair stators equipped with the proposed seven-phase winding layouts, and the simulation results are shown in Figs. 7(a) and (b), respectively. Clearly, the 24-slot stator phase currents are closer to the ideal seven-phase case, where all phases should perfectly be balanced.

3) ELEVEN-PHASE CASE

The last considered case has an eleven-phase stator winding. Hence, the MMF harmonics are mapped to five subspaces, namely, $\alpha\beta$, xy_1, xy_2, xy_3, and xy_4. These subspaces comprise the fundamental, third, fifth, seventh, and ninth space harmonic orders, respectively. As a matter of fact, in multiphase machines, the MMF distribution becomes more sinusoidal as the number of phases increases. Using 22-slot and 24-slot stators for the conventional and the proposed eleven-phase winding layouts, respectively, Fig. 8 proves that the conventional, as well as the proposed eleven-phase winding, are quite similar. Very small coupling is obtained for the xy_3 and xy_4 subspaces, while the main effective subspaces ($\alpha\beta$, xy_1, and xy_2) are fairly decoupled. The FEA results for the stator currents under rated conditions are shown in Fig. 9, which indicates approximately balanced currents. The very small unbalance component is mainly due to the difference in the mutual leakage inductance between phases, as will mathematically be verified later.

In a nutshell, the magnetizing flux distributions and their sequence components of the proposed winding layouts are quite similar to the conventional symmetrical n-phase cases provided that the number of stator slots will be close enough to standard n-phase stators. This proves that the magnetizing flux produced by the proposed winding layouts can be perfectly decomposed using VSD, which allows for the same VSD-based controllers employed in conventional n-phase cases. For the same total number of turns, the machine

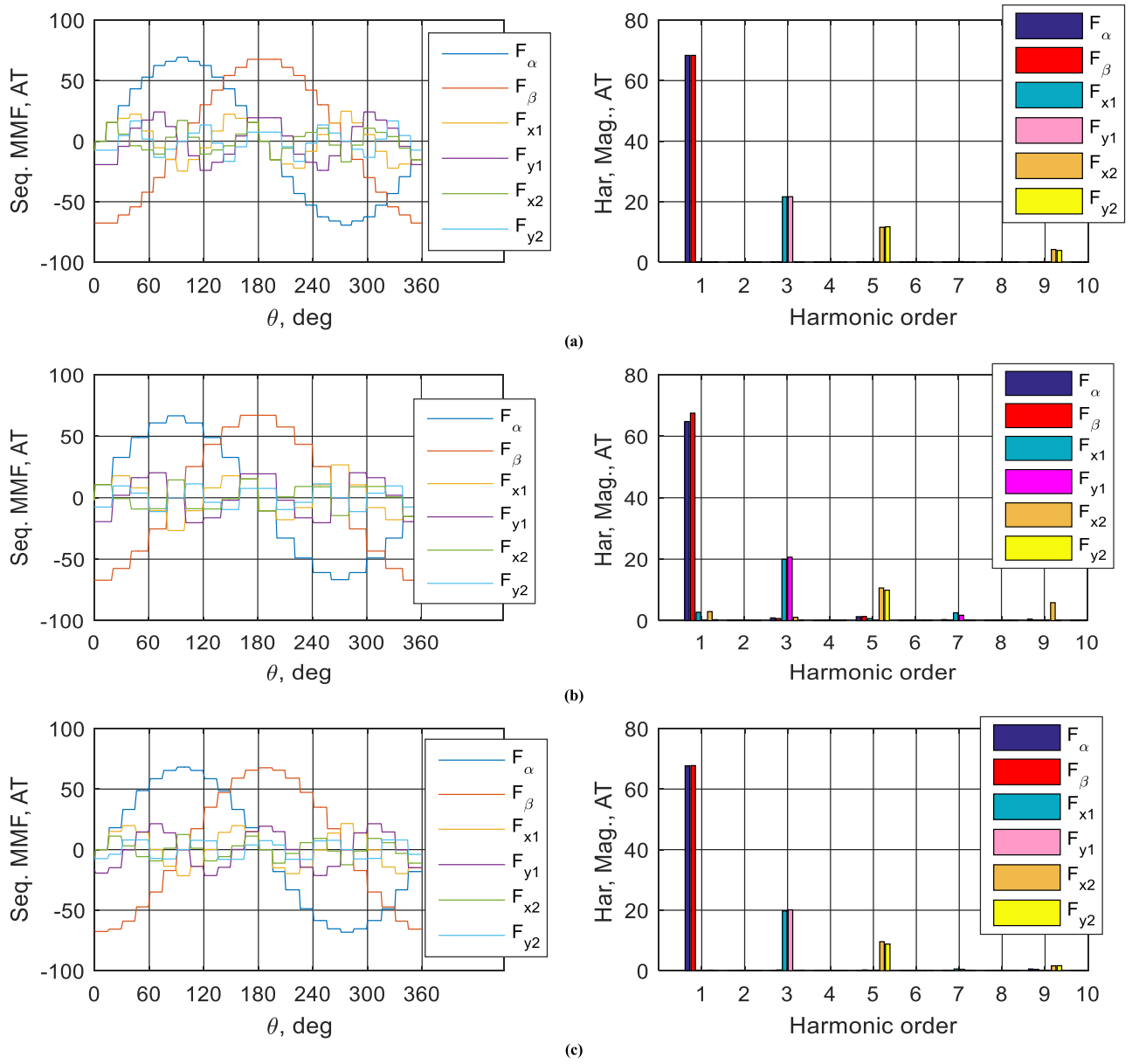

FIGURE 6. MMF sequence components for the seven-phase case. (a) Conventional seven-phase stator using 28-slot stator. (b) Proposed seven-phase winding using 18-slot stator. (c) Proposed seven-phase winding using 24-slot stator.

magnetizing inductances of different subspaces of the conventional and the proposed winding layouts will, therefore, be the same.

B. SEQUENCE COMPONENTS OF STATOR LEAKAGE FLUX

Generally, the stator winding leakage inductance comprises three components, namely, slot, end-coil, and air-gap leakage components. The air-gap leakage component mainly represents the effect of the spatial harmonics of the air gap MMF [24]. Since the harmonic mapping was proven to be the same as the conventional n-phase winding, this leakage inductance term will be similar to the conventional case. The same is also expected for the end-coil inductance since the medium is air with the same permeance. The main concern will, therefore, be with the slot leakage inductance, where the sequence mutual leakage inductance will vary from subspace to another [25].

For a double layer winding, the total slot leakage flux linkage, λ_{sl}, of each coil comprises three components due to the upper (top), lower (bottom) coil side fluxes, and the mutual flux between them, and can therefore be put in the following form:

$$\lambda_{sl} = N_{ct}^2 P_t i_t + N_{cb}^2 P_b i_b + 2N_{ct} N_{cb} P_{tb} i_t i_b \qquad (2)$$

where, P_t, P_b, and P_{tb} are the total slot permeances associated with the top conductors, bottom conductors, and mutual

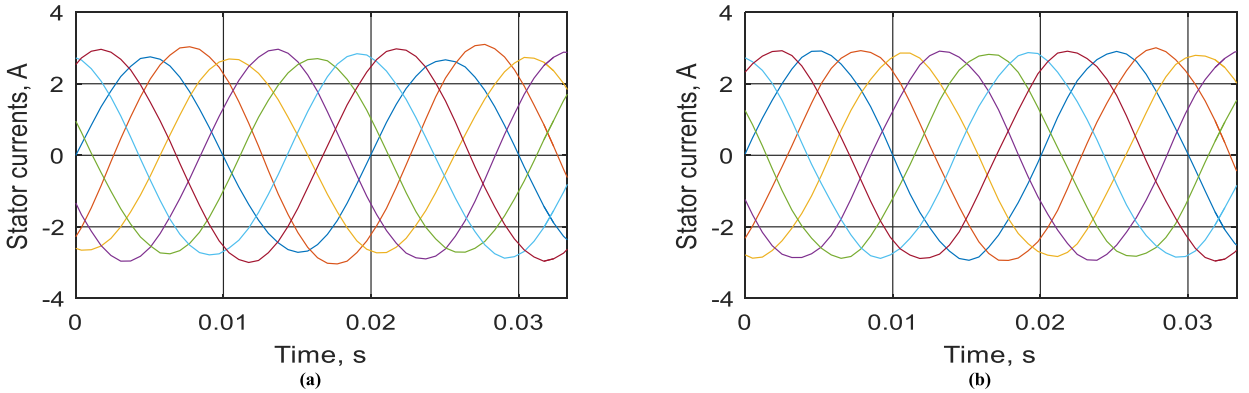

FIGURE 7. FE simulation results for the seven-phase stator phase currents. (a) 18-slot stator. (b) 24-slot stator.

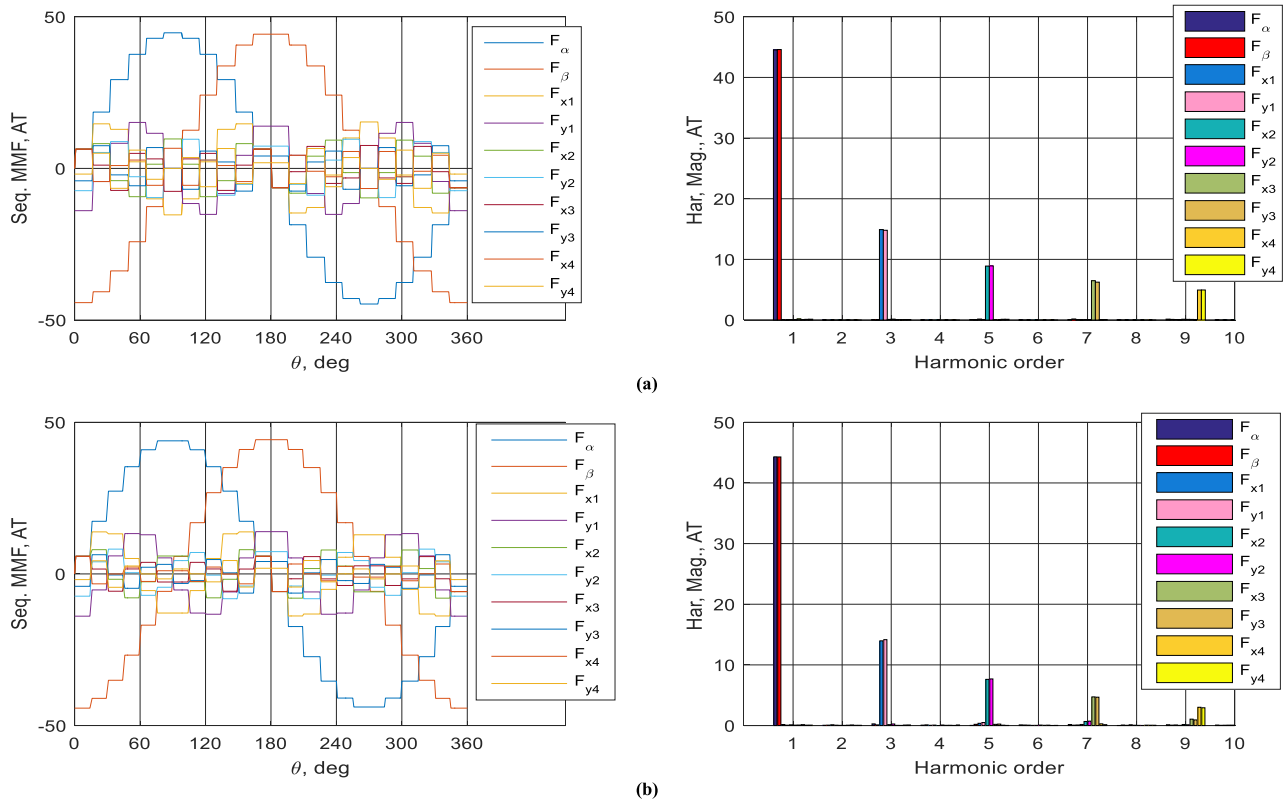

FIGURE 8. MMF sequence components for the eleven-phase case. (a) Conventional eleven-phase stator using 22-slot stator. (b) Proposed eleven-phase winding using 24-slot stator.

coupling between the two layers, respectively; N_{ct}, N_{cb} are the number of conductors in the upper and lower layers, respectively.

The relation between these permeances highly depends on the slot shape [25].

In the following analysis, the stator leakage inductance matrices are calculated for the same previously considered cases in subsection III.A. For the proposed winding layouts, each slot generally comprises coils with different numbers of turns. In order to simplify the mathematical formulation, the number of conductors comprising each slot is assumed to be equally divided between the two layers. This is carried out by splitting the coil sides having a larger number of turns into two portions such that the number of conductors in both layers will eventually be equal. This will allow the employment of the calculation technique for leakage inductance given in [25].

1) FIVE-PHASE CASE

For the 18-slot five-phase winding layout given in Fig. 1, the distribution of the conductors between the two layers can be rearranged, as shown in the layout given in Fig. 10,

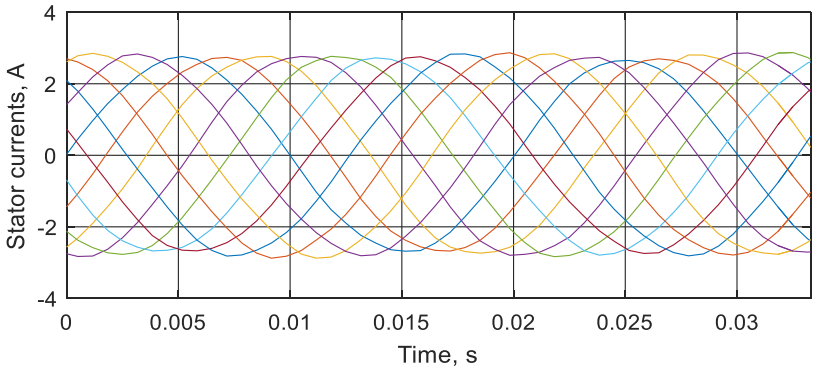

FIGURE 9. FE simulation results for the 24-slot eleven-phase stator phase currents.

Phase (j)		a	b	c	d	e				
Slot (i)		1	2	3	4	5	6	7	8	9
$\frac{N_{ij}}{N_c}$	U	a(0.6)	-d(0.2) a(0.4)	-d(0.5)	b(0.4) -d(0.2)	b(0.5)	-e(0.6)	-e(0.5)	c(0.6)	c(0.5)
	L	a(0.4) -c(0.2)	a(0.6)	-d(0.5)	-d(0.6)	b(0.5)	b(0.6)	-e(0.5)	c(0.2) -e(0.4)	c(0.5)

FIGURE 10. 18-slot/2-pole five-phase winding layout with conductors per slots divided into two equal layers.

to ensure an equal number of conductors per layer. Based on this distribution of different conductors per slot, the total leakage flux for *phase a* can be calculated using (2) is given by (3).

$$\begin{aligned}\lambda_{lsa} = N_c^2 \Big\{ & P_t \left(0.6^2 + 0.4^2 + 0.6^2 + 0.4^2\right) \\ & + P_b \left(0.6^2 + 0.4^2 + 0.6^2 + 0.4^2\right) \\ & + 2P_{tb}(0.6 \times 0.4 + 0.6 \times 0.4)\} \cdot i_a \\ & - 2N_c^2 P_{tb}(0.2 \times 1) \cdot i_c - 2N_c^2 P_{tb}(0.2 \times 1) \cdot i_d \end{aligned} \quad (3)$$

where N_c is the number of conductors per slot for the original three-phase stator.

This can be reduced to;

$$\begin{aligned}\lambda_{lsa} = N_c^2 \left(1.04P_t + 1.04P_b + 0.96P_{tb}\right) \\ i_a - 0.4N_c^2 P_{tb} i_c - 0.4N_c^2 P_{tb} i_d \end{aligned} \quad (4)$$

Similarly, for *phase b*, the slot leakage flux is given by;

$$\begin{aligned}\lambda_{lsb} = N_c^2 \Big\{ & P_t \left(0.4^2 + 0.5^2 + 0.5^2 + 0.6^2\right) \\ & + P_b \left(0.4^2 + 0.5^2 + 0.5^2 + 0.6^2\right) \\ & + 2P_{tb}(0.5 \times 0.5)\} \cdot i_b \\ & - 2N_c^2 P_{tb}(0.4 \times 0.8) \cdot i_d - 2N_c^2 P_{tb}(0.6 \times 0.6) \cdot i_e \end{aligned} \quad (5)$$

Which can be reduced to:

$$\begin{aligned}\lambda_{lsb} = N_c^2 \left(1.02P_t + 1.02P_b + 0.5P_{tb}\right) i_b \\ - 0.64N_c^2 P_{tb} i_d - 0.72N_c^2 P_{tb} i_e \end{aligned} \quad (6)$$

Following the same concept for *phases c*, *d*, and *e*, the corresponding slot leakage fluxes are given by (7), (8), and (9), respectively.

$$\begin{aligned}\lambda_{lsc} = & N_c^2 \left(0.94P_t + 0.94P_b + 0.74P_{tb}\right) i_c \\ & - 0.4N_c^2 P_{tb} i_a - 0.64N_c^2 P_{tb} i_e \end{aligned} \quad (7)$$

$$\begin{aligned}\lambda_{lsd} = & N_c^2 \left(0.94P_t + 0.94P_b + 0.74P_{tb}\right) i_d \\ & - 0.4N_c^2 P_{tb} i_a - 0.64N_c^2 P_{tb} i_b \end{aligned} \quad (8)$$

$$\begin{aligned}\lambda_{lse} = & N_c^2 \left(1.02P_t + 1.02P_b + 0.5P_{tb}\right) i_e \\ & - 0.72N_c^2 P_{tb} i_b - 0.64N_c^2 P_{tb} i_c \end{aligned} \quad (9)$$

The stator phase leakage flux vector $\left[\lambda_{ls}^{ph}\right] = [\lambda_{lsa}\ \lambda_{lsb}\ \lambda_{lsc}\ \lambda_{lsd}\ \lambda_{lse}]^T$, can be expressed as a function of the phase current vector, $\left[i_s^{ph}\right] = \left[\, i_a\ i_b\ i_c\ i_d\ i_e \,\right]^T$, as follows:

$$\left[\lambda_{ls}^{ph}\right] = \left[L_{ls}^{ph}\right]\left[i_s^{ph}\right] + \left[L_{lm}^{ph}\right]\left[i_s^{ph}\right] \quad (10)$$

where the self-leakage and mutual-leakage stator phase inductance matrices $\left[L_{ls}^{ph}\right]$ and $\left[L_{lm}^{ph}\right]$, respectively, are given by (11) and (12).

$$\left[L_{ls}^{ph(prop.)}\right] = N_c^2 \left(P_t + P_b\right) \times \begin{bmatrix} 1.04 & 0 & 0 & 0 & 0 \\ 0 & 1.02 & 0 & 0 & 0 \\ 0 & 0 & 0.94 & 0 & 0 \\ 0 & 0 & 0 & 0.94 & 0 \\ 0 & 0 & 0 & 0 & 1.02 \end{bmatrix} \quad (11)$$

$$\left[L_{lm}^{ph(prop.)}\right] = N_c^2 P_{tb} \times \begin{bmatrix} 0.96 & 0 & -0.4 & -0.4 & 0 \\ 0 & 0.5 & 0 & -0.64 & -0.72 \\ -0.4 & 0 & 0.74 & 0 & -0.64 \\ -0.4 & -0.64 & 0 & 0.74 & 0 \\ 0 & -0.72 & -0.64 & 0 & 0.5 \end{bmatrix} \tag{12}$$

By applying (1) with $n = 5$, the corresponding sequence components, after discarding the zero-sequence component, are given by,

$$\begin{bmatrix} \lambda_\alpha^{ls} \\ \lambda_\beta^{ls} \\ \lambda_x^{ls} \\ \lambda_y^{ls} \end{bmatrix} = l_s \begin{bmatrix} 1 & 0 & 0.024 & 0 \\ 0 & 1.01 & 0 & 0.036 \\ 0.024 & 0 & 1.04 & 0 \\ 0 & 0.036 & 0 & 0.98 \end{bmatrix} \begin{bmatrix} i_{\alpha s} \\ i_{\beta s} \\ i_{xs} \\ i_{ys} \end{bmatrix} + l_m \begin{bmatrix} 1 & 0 & 0.037 & 0 \\ 0 & 1.086 & 0 & 0.047 \\ 0.037 & 0 & 0.251 & 0 \\ 0 & 0.047 & 0 & 0.196 \end{bmatrix} \begin{bmatrix} i_{\alpha s} \\ i_{\beta s} \\ i_{xs} \\ i_{ys} \end{bmatrix} \tag{13}$$

where $l_s = 0.9861 N_c^2 (P_t + P_b)$, $l_m = 1.5284 N_c^2 P_{tb}$.

It is clear that for each subspace, there is no cross-coupling between its components. Also, the mutual coupling between different subspaces is less than 4%, which may be assumed negligible, with the fact that the contribution of secondary subspaces can merely be neglected [23]. Also, the $\alpha\beta$ inductance terms (represented by the red dashed boxes) are very close for the self-leakage inductance term, and with an approximately 8.6% mismatch in the $\alpha\beta$ mutual leakage inductances term. Generally, the contribution of the mutual leakage inductance to the total stator leakage inductance depends on the slot design. Similar to the definition made in [25], the coefficient k_{mtb}, which represents the ratio between the mutual- and self-leakage inductance terms, is defined as follows,

$$k_{mtb}^{prop.} = \frac{l_m}{l_s} = 1.55 \frac{P_{tb}}{(P_t + P_b)} \tag{14}$$

It has been clarified in [25] that the coefficient k_{mtb} varies from 0.25 to 0.35 for open slots, while it may increase up to 0.5 in semi-closed slot shapes. The coefficient k_{mtb} equals zero in single layer windings.

For the sake of comparison with the standard case, the calculated inductance matrix for a 20-slot standard five-phase stator is also given assuming the same total number of conductors. To have a meaningful comparison and to show the effect of the mutual leakage inductance on VSD of phase values, a double layer winding is assumed for the symmetrical five-phase case to show the expected value for the coefficient k_{mtb} in standard five-phase winding having same slot design. The winding is assumed to be chorded with one slot to justify a double layer winding. Following the same previous technique, the leakage phase inductance matrices are given by;

$$\left[L_{ls}^{ph(Conv.)}\right] = N_c^2 (P_t + P_b) \times \begin{bmatrix} 1 & 0 & 0 & 0 & 0 \\ 0 & 1 & 0 & 0 & 0 \\ 0 & 0 & 1 & 0 & 0 \\ 0 & 0 & 0 & 1 & 0 \\ 0 & 0 & 0 & 0 & 1 \end{bmatrix} \tag{15}$$

$$\left[L_{lm}^{ph(Conv.)}\right] = N_c^2 P_{tb} \times \begin{bmatrix} 0.5 & 0 & -0.5 & -0.5 & 0 \\ 0 & 0.5 & 0 & -0.5 & -0.5 \\ -0.5 & 0 & 0.5 & 0 & -0.5 \\ -0.5 & -0.5 & 0 & 0.5 & 0 \\ 0 & -0.5 & -0.5 & 0 & 0.5 \end{bmatrix} \tag{16}$$

By applying (1), the corresponding sequence components are given by:

$$\begin{bmatrix} \lambda_\alpha^{ls} \\ \lambda_\beta^{ls} \\ \lambda_x^{ls} \\ \lambda_y^{ls} \end{bmatrix} = l_s^{conv.} \begin{bmatrix} 1 & 0 & 0 & 0 \\ 0 & 1 & 0 & 0 \\ 0 & 0 & 1 & 0 \\ 0 & 0 & 0 & 1 \end{bmatrix} \begin{bmatrix} i_{\alpha s} \\ i_{\beta s} \\ i_{xs} \\ i_{ys} \end{bmatrix} + l_m^{conv.} \begin{bmatrix} 1 & 0 & 0 & 0 \\ 0 & 1 & 0 & 0 \\ 0 & 0 & 0.146 & 0 \\ 0 & 0 & 0 & 0.146 \end{bmatrix} \begin{bmatrix} i_{\alpha s} \\ i_{\beta s} \\ i_{xs} \\ i_{ys} \end{bmatrix} \tag{17}$$

where $l_s^{conv.} = N_c^2 (P_t + P_b)$, $l_m^{conv.} = 1.31 N_c^2 P_{tb}$.

The coefficient k_{mtb} for this winding is then calculated as:

$$k_{mtb}^{conv.} = 1.31 \frac{P_{tb}}{(P_t + P_b)} \tag{18}$$

Clearly, the proposed winding can effectively approximate this ideal five-phase case. However, the coefficient k_{mtb} of the 18-slot five-phase winding seems to be approximately 18% higher. This means that the effect of the mutual leakage inductance will be higher. Nevertheless, this slight increase has nothing to do with the machine dynamic response, while it will likely decrease the maximum pullout torque, a well-known fact for multiphase machines with a double layer winding [26], [27]. On the other hand, the effect of the small unbalance in the $\alpha\beta$ components of the stator leakage inductance on the machine dynamic response as well as the phase currents magnitude diversion will be shown in a subsequent section.

2) SEVEN-PHASE CASE

The stator winding inductance matrices of the 18-slot and 24-slot stators shown in Figs. 2 and 3 will be compared with a standard 28-slot seven-phase stator.

i) 18-slot stator:

The winding layout shown in Fig. 2 can be rearranged, as shown in Fig. 11, to allow for an equal number of conductors between the upper and the lower layers. Following the

Phase (j)		a	b	c	d	e	f	g		
Slot		1	2	3	4	5	6	7	8	9
$\frac{N_{ij}}{N_c}$	U	a (0.43)	-e (0.4)	b (0.365)	-f (0.15) b (0.215)	-f (0.43)	c (0.43)	-g (0.365)	d (0.29) -g (0.075)	-a (0.08) d (0.32)
	L	a (0.43)	-e (0.32) a (0.08)	b (0.075) -e (0.29)	b (0.365)	-f (0.43)	c (0.43)	-g (0.215) c (0.15)	-g (0.365)	d (0.4)

FIGURE 11. 18-slot/2-pole seven-phase winding layout with conductors per slots divided into two equal layers.

same concept, the stator leakage flux vector $\left[\lambda_{ls}^{ph}\right]$ between different phases can then be written as given by (19), as shown at the bottom of this page. By applying (1) with $n = 7$, the corresponding sequence components, are given by (20), as shown at the bottom of this page. The coefficient k_{mtb} is then calculated as given by (21). where, $l_s = 0.3518N_c^2(P_t + P_b)$, $l_m = 0.6238N_c^2P_{tb}$.

$$k_{mtb} = \frac{l_m}{l_s} = 1.773\frac{P_{tb}}{(P_t + P_b)} \tag{21}$$

For this slot number, the mutual leakage flux yields a higher coupling between subspaces, which complies with the previous conclusion regarding the magnetizing flux for the same stator slot number (18-slot/pole-pair). This coupling will give rise to a certain degree of unbalance between phases, however, its effect on the torque production, and hence, the system dynamics can still be tolerated.

ii) 24-slot stator:

The winding given in Fig. 3 is rearranged in two equal layers, as shown in Fig. 12. This slot number is closer to a conventional 28-slot seven-phase stator. Hence, the decomposed sequence inductance matrix will expectedly be much better than the previously presented 18-slot stator case.

The calculated stator leakage flux vector and its sequence components are then given by (22) and (23), as shown at the top of the next page, respectively.

$$\begin{bmatrix}\lambda_{lsa}\\ \lambda_{lsb}\\ \lambda_{lsc}\\ \lambda_{lsd}\\ \lambda_{lse}\\ \lambda_{lsf}\\ \lambda_{lsg}\end{bmatrix} = N_c^2(P_t + P_b)\begin{bmatrix}0.3826 & 0 & 0 & 0 & 0 & 0 & 0\\ 0 & 0.3183 & 0 & 0 & 0 & 0 & 0\\ 0 & 0 & 0.3923 & 0 & 0 & 0 & 0\\ 0 & 0 & 0 & 0.3465 & 0 & 0 & 0\\ 0 & 0 & 0 & 0 & 0.3645 & 0 & 0\\ 0 & 0 & 0 & 0 & 0 & 0.3926 & 0\\ 0 & 0 & 0 & 0 & 0 & 0 & 0.3183\end{bmatrix}\begin{bmatrix}i_{sa}\\ i_{sb}\\ i_{sc}\\ i_{sd}\\ i_{se}\\ i_{sf}\\ i_{sg}\end{bmatrix}$$
$$+N_c^2P_{tb}\begin{bmatrix}0.3698 & 0 & 0 & -0.1152 & -0.1152 & 0 & 0\\ 0 & 0.2117 & 0 & 0 & -0.2552 & -0.174 & 0\\ 0 & 0 & 0.3698 & 0 & 0 & 0 & -0.174\\ -0.1152 & 0 & 0 & 0.256 & 0 & 0 & -0.2552\\ -0.1152 & -0.2552 & 0 & 0 & 0.256 & 0 & 0\\ 0 & -0.174 & 0 & 0 & 0 & 0.3698 & 0\\ 0 & 0 & -0.174 & -0.2552 & 0 & 0 & 0.2117\end{bmatrix}\begin{bmatrix}i_{sa}\\ i_{sb}\\ i_{sc}\\ i_{sd}\\ i_{se}\\ i_{sf}\\ i_{sg}\end{bmatrix} \tag{19}$$

$$\begin{bmatrix}\lambda_{\alpha}^{ls}\\ \lambda_{\beta}^{ls}\\ \lambda_{x1}^{ls}\\ \lambda_{y1}^{ls}\\ \lambda_{x2}^{ls}\\ \lambda_{y2}^{ls}\end{bmatrix} = \left(l_s\begin{bmatrix}1 & 0 & 0.04 & 0 & 0.05 & 0\\ 0 & 1.03 & 0 & -0.07 & 0 & 0.06\\ 0.04 & 0 & 1.01 & 0 & -0.02 & 0\\ 0 & -0.07 & 0 & 1.02 & 0 & 0.01\\ 0.05 & 0 & -0.02 & 0 & 1.07 & 0\\ 0 & 0.06 & 0 & -0.01 & 0 & 0.96\end{bmatrix}\right.$$
$$\left.+l_m\begin{bmatrix}1 & -0.15 & -0.17 & 0.14 & 0.19 & -0.06\\ -0.05 & 1.08 & 0.126 & -0.06 & -0.18 & 0.11\\ -0.11 & 0.235 & 0.75 & -0.167 & -0.265 & 0.115\\ -0.025 & 0.21 & 0.07 & 0.468 & -0.101 & 0.039\\ 0.054 & 0.064 & -0.005 & -0.029 & 0.352 & 0.038\\ 0.056 & -0.225 & -0.158 & 0.188 & 0.228 & -0.209\end{bmatrix}\right)\begin{bmatrix}i_{\alpha s}\\ i_{\beta s}\\ i_{xs1}\\ i_{ys1}\\ i_{xs2}\\ i_{ys2}\end{bmatrix} \tag{20}$$

$$\begin{bmatrix}\lambda_{sla}\\ \lambda_{slb}\\ \lambda_{slc}\\ \lambda_{sld}\\ \lambda_{sle}\\ \lambda_{slf}\\ \lambda_{slg}\end{bmatrix} = N_c^2\,(P_t+P_b)\begin{bmatrix}0.574 & 0 & 0 & 0 & 0 & 0 & 0\\ 0 & 0.6156 & 0 & 0 & 0 & 0 & 0\\ 0 & 0 & 0.59805 & 0 & 0 & 0 & 0\\ 0 & 0 & 0 & 0.61245 & 0 & 0 & 0\\ 0 & 0 & 0 & 0 & 0.61245 & 0 & 0\\ 0 & 0 & 0 & 0 & 0 & 0.59805 & 0\\ 0 & 0 & 0 & 0 & 0 & 0 & 0.6156\end{bmatrix}\begin{bmatrix}i_{sa}\\ i_{sb}\\ i_{sc}\\ i_{sd}\\ i_{se}\\ i_{sf}\\ i_{sg}\end{bmatrix}$$
$$N_c^2P_{tb}\begin{bmatrix}0.47 & 0 & 0 & -0.4104 & -0.4104 & 0 & 0\\ 0 & 0.3042 & 0 & 0 & -0.504 & -0.4356 & 0\\ 0 & 0 & 0.46035 & 0 & 0 & -0.3744 & -0.4356\\ -0.4104 & 0 & 0 & 0.35795 & 0 & 0 & -0.504\\ -0.4104 & -0.504 & 0 & 0 & 0.35795 & 0 & 0\\ 0 & -0.4356 & -0.3744 & 0 & 0 & 0.46035 & 0\\ 0 & 0 & -0.4356 & -0.504 & 0 & 0 & 0.3042\end{bmatrix}\begin{bmatrix}i_{sa}\\ i_{sb}\\ i_{sc}\\ i_{sd}\\ i_{se}\\ i_{sf}\\ i_{sg}\end{bmatrix} \quad (22)$$

$$\begin{bmatrix}\lambda_{\alpha}^{ls}\\ \lambda_{\beta}^{ls}\\ \lambda_{x1}^{ls}\\ \lambda_{y1}^{ls}\\ \lambda_{x2}^{ls}\\ \lambda_{y2}^{ls}\end{bmatrix} = \left(l_s\begin{bmatrix}1 & 0 & -0.018 & 0 & -0.021 & 0\\ 0 & 1.007 & 0 & 0.011 & 0 & -0.01\\ -0.018 & 0 & 1 & 0 & -0.01 & 0\\ 0 & 0.011 & 0 & 1.01 & 0 & 0.003\\ -0.021 & 0 & -0.01 & 0 & 0.99 & 0\\ 0 & -0.01 & 0 & 0.003 & 0 & 1.02\end{bmatrix}\right.$$
$$\left. + l_m\begin{bmatrix}1 & 0 & -0.005 & 0 & 0.024 & 0\\ 0 & 0.99 & 0 & 0.007 & 0 & 0.03\\ -0.005 & 0 & 0.484 & 0 & 0 & 0\\ 0 & 0 & 0 & 0.5 & 0 & -0.016\\ 0.024 & 0 & 0 & 0 & -0.04 & 0\\ 0 & 0.034 & 0 & -0.016 & 0 & -0.227\end{bmatrix}\right)\begin{bmatrix}i_{\alpha s}\\ i_{\beta s}\\ i_{xs1}\\ i_{ys1}\\ i_{xs2}\\ i_{ys2}\end{bmatrix} sss \quad (23)$$

where $l_s = 0.6018N_c^2\,(P_t+P_b)$, $l_m = 1.1855N_c^2P_{tb}$

$$k_{mtb} = \frac{l_m}{l_s} = 1.97\frac{P_{tb}}{(P_t+P_b)} \quad (24)$$

$$\begin{bmatrix}\lambda_{\alpha}^{ls}\\ \lambda_{\beta}^{ls}\\ \lambda_{x1}^{ls}\\ \lambda_{y1}^{ls}\\ \lambda_{x2}^{ls}\\ \lambda_{y2}^{ls}\end{bmatrix} = l_s^{conv.}\begin{bmatrix}1 & 0 & 0 & 0 & 0 & 0\\ 0 & 1 & 0 & 0 & 0 & 0\\ 0 & 0 & 1 & 0 & 0 & 0\\ 0 & 0 & 0 & 1 & 0 & 0\\ 0 & 0 & 0 & 0 & 1 & 0\\ 0 & 0 & 0 & 0 & 0 & 1\end{bmatrix}\begin{bmatrix}i_{\alpha s}\\ i_{\beta s}\\ i_{xs1}\\ i_{ys1}\\ i_{xs2}\\ i_{ys2}\end{bmatrix} + l_m^{conv.}\begin{bmatrix}1 & 0 & 0 & 0 & 0 & 0\\ 0 & 1 & 0 & 0 & 0 & 0\\ 0 & 0 & 0.516 & 0 & 0 & 0\\ 0 & 0 & 0 & 0.516 & 0 & 0\\ 0 & 0 & 0 & 0 & -0.09 & 0\\ 0 & 0 & 0 & 0 & 0 & -0.09\end{bmatrix}\begin{bmatrix}i_{\alpha s}\\ i_{\beta s}\\ i_{xs1}\\ i_{ys1}\\ i_{xs2}\\ i_{ys2}\end{bmatrix} \quad (25)$$

where $l_s^{conv.} = N_c^2\,(P_t+P_b)$, $l_m^{conv.} = 1.4N_c^2P_{tb}$

$$k_{mtb} = \frac{l_m}{l_s} = 1.4\frac{P_{tb}}{(P_t+P_b)} \quad (26)$$

For this winding layout, the coefficient k_{mtb} is then calculated by (24), as shown at the top of this page. Clearly, this case is much better than the 18-slot stator in terms of coupling between different subspaces as well as unbalance in the $\alpha\beta$ leakage inductance components. The obtained coupling due to the uneven winding distribution is less than 4%, which agrees with the same conclusion made for the five-phase case with an 18-slot stator.

Similar to the five-phase case, the conventional seven-phase stator, having 28 slots with coils chorded by one slot, corresponds to the sequence leakage inductance matrices given by (25), as shown at the top of this page, and k_{mtb} coefficient is given by (26), as shown at the top of this page.

By comparing the conventional and the proposed windings, the 24-slot stator has less unbalance in the inductance sequence component; however, it corresponds to a higher contribution of the mutual leakage inductance to the total stator leakage inductance.

3) ELEVEN-PHASE CASE

The 24-slot eleven-phase winding layout shown in Fig. 4 is rearranged in two layers with an equal number of conductors,

$$
\begin{bmatrix} \lambda_{lsa} \\ \lambda_{lsb} \\ \lambda_{lsc} \\ \lambda_{lsc} \\ \lambda_{lse} \\ \lambda_{lse} \\ \lambda_{lsg} \\ \lambda_{lsg} \\ \lambda_{lsk} \\ \lambda_{lsk} \end{bmatrix} = N_c^2 (P_t + P_b) \begin{bmatrix} 0.419 & 0 & 0 & 0 & 0 & 0 & 0 & 0 & 0 & 0 & 0 \\ 0 & 0.377 & 0 & 0 & 0 & 0 & 0 & 0 & 0 & 0 & 0 \\ 0 & 0 & 0.381 & 0 & 0 & 0 & 0 & 0 & 0 & 0 & 0 \\ 0 & 0 & 0 & 0.431 & 0 & 0 & 0 & 0 & 0 & 0 & 0 \\ 0 & 0 & 0 & 0 & 0.363 & 0 & 0 & 0 & 0 & 0 & 0 \\ 0 & 0 & 0 & 0 & 0 & 0.425 & 0 & 0 & 0 & 0 & 0 \\ 0 & 0 & 0 & 0 & 0 & 0 & 0.425 & 0 & 0 & 0 & 0 \\ 0 & 0 & 0 & 0 & 0 & 0 & 0 & 0.363 & 0 & 0 & 0 \\ 0 & 0 & 0 & 0 & 0 & 0 & 0 & 0 & 0.431 & 0 & 0 \\ 0 & 0 & 0 & 0 & 0 & 0 & 0 & 0 & 0 & 0.381 & 0 \\ 0 & 0 & 0 & 0 & 0 & 0 & 0 & 0 & 0 & 0 & 0.377 \end{bmatrix}
$$

$$
\times \begin{bmatrix} i_{sa} \\ i_{sb} \\ i_{sc} \\ i_{sd} \\ i_{se} \\ i_{se} \\ i_{s}f \\ i_{s}i \\ i_{si} \\ i_{sk} \\ i_{sk} \end{bmatrix}
$$

$$
+ N_c^2 P_t \begin{bmatrix} 0.414 & 0 & 0 & 0 & 0 & -0.091 & -0.091 & 0 & 0 & 0 & 0 \\ 0 & 0 & 0 & 0 & 0 & 0 & -0.164 & -0.277 & 0 & 0 & 0 \\ 0 & 0 & 0 & 0 & 0 & 0 & 0 & -0.358 & -0.407 & 0 & 0 \\ 0 & 0 & 0 & 0 & 0 & 0 & 0 & 0 & -0.423 & -0.407 & 0 \\ 0 & 0 & 0 & 0 & 0 & 0 & 0 & 0 & 0 & -0.358 & -0.277 \\ -0.091 & 0 & 0 & 0 & 0 & 0 & 0 & 0 & 0 & 0 & -0.164 \\ -0.091 & -0.164 & 0 & 0 & 0 & 0 & 0 & 0 & 0 & 0 & 0 \\ 0 & -0.277 & -0.358 & 0 & 0 & 0 & 0 & 0 & 0 & 0 & 0 \\ 0 & 0 & -0.407 & -0.423 & 0 & 0 & 0 & 0 & 0 & 0 & 0 \\ 0 & 0 & 0 & -0.407 & -0.358 & 0 & 0 & 0 & 0 & 0 & 0 \\ 0 & 0 & 0 & 0 & -0.277 & -0.164 & 0 & 0 & 0 & 0 & 0 \end{bmatrix}
$$

$$
\times \begin{bmatrix} i_{sa} \\ i_{sb} \\ i_{sc} \\ i_{sd} \\ i_{se} \\ i_{se} \\ i_{sg} \\ i_{sg} \\ i_{sg} \\ i_{s}j \\ i_{sk} \end{bmatrix} \tag{27}
$$

Phase (j)		a	b	c	d	e	f	g					
Slot		1	2	3	4	5	6	7	8	9	10	11	12
$\frac{N_{ij}}{N_c}$	U	a (0.47)	-e (0.22)	-e (0.42)	b (0.45)	b (0.39)	-f (0.495)	c (0.12)	c (0.45)	-g (0.33)	-g (0.39)	d (0.505)	-a (0.06)
			a (0.25)		-e (0.055)			-f (0.33)		c (0.165)			d (0.36)
	L	a (0.25)	a (0.47)	-e (0.36)	-e (0.505)	b (0.39)	-f (0.165)	-f (0.45)	c (0.33)	c (0.495)	-g (0.39)	d(0.055)	d (0.42)
		-d (0.22)		a (0.06)			b (0.33)		-f (0.12)			-g (0.45)	

FIGURE 12. 24-slot/2-pole seven-phase winding layout with conductors per slots divided into two equal layers.

Phase (j)		a	b	c	d	e	f	g	h	i	j	k	
Slot		1	2	3	4	5	6	7	8	9	10	11	12
$\frac{N_{ij}}{N_c}$	U	a (0.455)	-g (0.48)	b (0.46)	-h (0.46)	c (0.46)	-i (0.46)	d (0.46)	-j (0.37)	e (0.28)	-k (0.19)	f (0.1)	-a (0.05)
									d (0.09)	-j (0.18)	e (0.27)	-k (0.36)	f (0.43)
	L	a (0.455)	-g (0.43)	b(0.36)	-h (0.27)	c (0.18)	-i (0.09)	-i (0.46)	d (0.46)	-j (0.46)	e (0.46)	-k (0.46)	f (0.48)
			a (0.05)	-g (0.1)	b (0.19)	-h (0.28)	c (0.37)						

FIGURE 13. 24-slot/2-pole eleven-phase winding layout with conductors per slots divided into two equal layers.

as shown in Fig. 13. The calculated stator leakage flux vector and the corresponding sequence vector are given by (27), as shown at the previous page, and (28), as shown at the bottom of this page, respectively, while, the coefficient k_{mtb} is given by (29), as shown at the bottom of this page. Although the uneven winding distribution introduces relatively higher

$$\begin{bmatrix} \lambda_{\alpha}^{ls} \\ \lambda_{\beta}^{ls} \\ \lambda_{\beta}^{ls} \\ \lambda_{x1}^{ls} \\ \lambda_{y1}^{ls} \\ \lambda_{x2}^{ls} \\ \lambda_{x3}^{ls} \\ \lambda_{x3}^{ls} \\ \lambda_{y4}^{ls} \\ \lambda_{y4}^{ls} \end{bmatrix} = l_s \begin{bmatrix} 1 & 0 & 0.05 & 0 & 0.034 & 0 & -0.013 & 0 & -0.01 & 0 \\ 0 & 0.992 & 0 & -0.04 & 0 & 0.056 & 0 & -0.0094 & 0 & 0.0083 \\ 0.05 & 0 & 0.985 & 0 & 0.003 & 0 & 0.04 & 0 & -0.02 & 0 \\ 0 & -0.04 & 0 & 1.007 & 0 & 0.006 & 0 & 0.0553 & 0 & 0.001 \\ 0.034 & 0 & 0.0025 & 0 & 0.986 & 0 & -0.006 & 0 & 0.0436 & 0 \\ 0 & 0.0564 & 0 & 0.0058 & 0 & 1.006 & 0 & 0.0141 & 0 & 0.047 \\ -0.013 & 0 & 0.04 & 0 & -0.006 & 0 & 0.994 & 0 & -0.007 & 0 \\ 0 & -0.009 & 0 & 0.0553 & 0 & 0.0141 & 0 & 0.998 & 0 & 0.015 \\ -0.01 & 0 & -0.02 & 0 & 0.04 & 0 & -0.007 & 0 & 1.04 & 0 \\ 0 & 0.008 & 0 & -0.001 & 0 & 0.047 & 0 & 0.015 & 0 & 0.951 \end{bmatrix} \begin{bmatrix} i_{\alpha s} \\ i_{\beta s} \\ i_{xs1} \\ i_{ys1} \\ i_{xs2} \\ i_{xs2} \\ i_{ys2} \\ i_{xs3} \\ i_{ys4} \end{bmatrix}$$

$$+ l_m \begin{bmatrix} 1 & 0 & -0.21 & 0 & 0.14 & 0 & 0.178 & 0 & 0.177 & 0 \\ 0 & 1.62 & 0 & -0.28 & 0 & -0.035 & 0 & -0.001 & 0 & 0 \\ -0.21 & 0 & 1 & 0 & 0.017 & 0 & 0.17 & 0 & 0.17 & 0 \\ 0 & -0.28 & 0 & 0.84 & 0 & -0.17 & 0 & 0.01 & 0 & 0.003 \\ 0.135 & 0 & 0.017 & 0 & 0.36 & 0 & 0.228 & 0 & 0.192 & 0 \\ 0 & -0.034 & 0 & -0.17 & 0 & 0.178 & 0 & 0.06 & 0 & 0.03 \\ 0.178 & 0 & 0.17 & 0 & 0.228 & 0 & -0.36 & 0 & 0.436 & 0 \\ 0 & 0.001 & 0 & -0.01 & 0 & 0.06 & 0 & 0.52 & 0 & 0.256 \\ 0.177 & 0 & 0.173 & 0 & 0.192 & 0 & 0.436 & 0-0.84 & 0 & \\ 0 & 0 & 0 & 0.003 & 0 & 0.03 & 0 & 0.256 & 0-1.13 & \end{bmatrix} \begin{bmatrix} i_{\alpha s} \\ i_{\beta s} \\ i_{xs1} \\ i_{ys1} \\ i_{xs2} \\ i_{xs2} \\ i_{xs3} \\ i_{xs4} \\ i_{ys4} \end{bmatrix} \quad (28)$$

where $l_s = 0.3993\, N_c^2\, (P_t + P_b)$, $l_m = 0.4315\, N_c^2 P_{tb}$

$$k_{mtb} = \frac{l_m}{l_s} = 1.08 \frac{P_{tb}}{(P_t + P_b)} \quad (29)$$

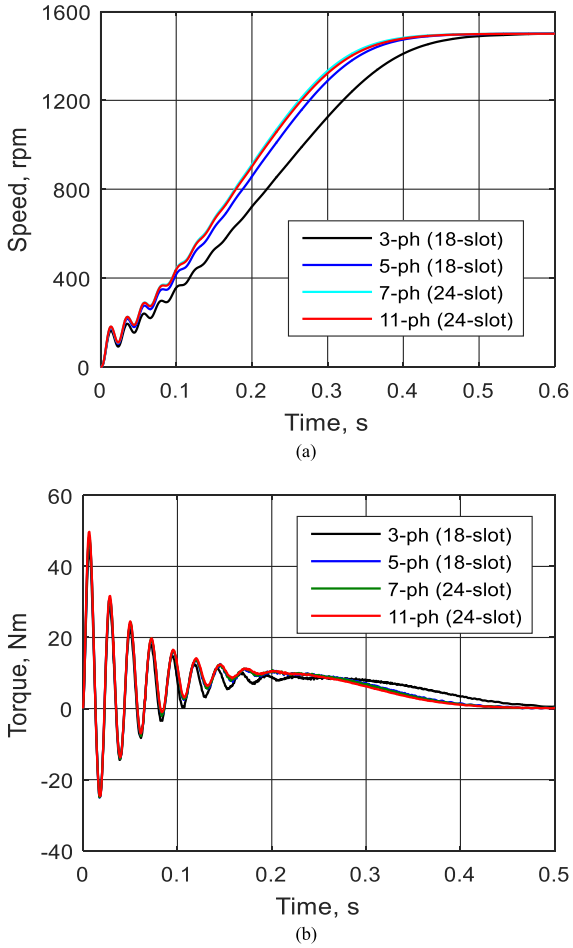

FIGURE 14. Direct online starting under different winding layouts. (a) Speed. (b) Torque.

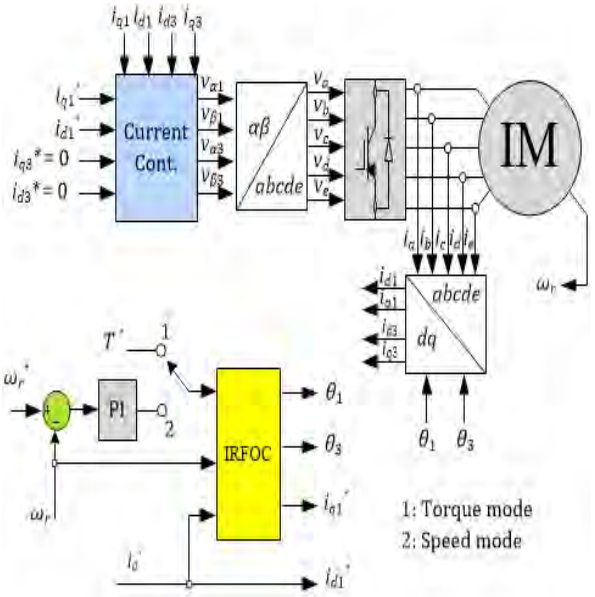

FIGURE 15. IRFOC controller of the five-phase IM.

coupling terms between subspaces and unbalanced $\alpha\beta$ mutual leakage inductances (as indicated by the second inductance matrix given by (28)), the cross-coupling terms for each subspace are still zero. The effect of this coupling will only appear as a small unbalance component between different phase currents, as will be confirmed later through simulations. Also, if $l_m < l_s$, which is the typical case for practical values of k_{mtb} , the effect of this unbalance may be insignificant.

It is worth noting that a conventional eleven-phase stator having 22-slot/pole pair can only be wound using a single layer winding which corresponds to a zero mutual-leakage inductance ($\boldsymbol{k_{mtb}= 0}$). To show the effect of a double-layer winding on the inductance matrix of a standard eleven-phase case, the number of slots should necessarily be increased. Hence, the comparison with the symmetrical winding will be discarded.

IV. EFFECT OF LEAKAGE INDUCTANCE MISMATCH ON THE DYNAMIC RESPONSE

Based on the provided analysis in section III, the proposed winding layouts will experience a certain degree of stator impedance mismatch, mainly due to the effect of the mutual component between the slot layers of the stator leakage flux. Nevertheless, it is a well-established fact in multiphase systems that torque production is mainly due to the fundamental subspace only. Therefore, the exploitation of the extra degrees of freedom offered by multiphase systems can ensure rated operating conditions even with some phases open [1]; the open-phase fault indeed corresponds to a completely asymmetric stator impedance matrix. It was also clear for all previously considered-cases that the $\alpha\beta$ leakage inductance terms are approximately equal for both the self-leakage and mutual leakage flux components (except for the eleven-phase case). The cross-coupling terms between the α and β axes are also too small to raise a concern. On the other hand, the mutual coupling with other subspaces will mainly give rise to some distortion in the current waveform (under core saturation), or yields phase current unbalance, similar to the presented study. Nevertheless, when all secondary subspace current components are properly controlled to zero, these parasitic effects will also be nullified. This is indeed a more resilient case than operating the machine under open phase conditions. Needless to say, the stator current asymmetry will inevitably happen in conventional symmetrical winding due to different winding/inverter asymmetries. The literature proved that this problem could simply be solved using current control without affecting the machine dynamic response. This is simply because the required secondary voltage components will generally be orthogonal with the torque producing voltage components.

In order to support the previous claim, a simulation case study using FEA is first introduced under free-running machine starting, with a step input applied voltage, to compare the dynamic response of the proposed winding layouts with the original three-phase winding using the same standard

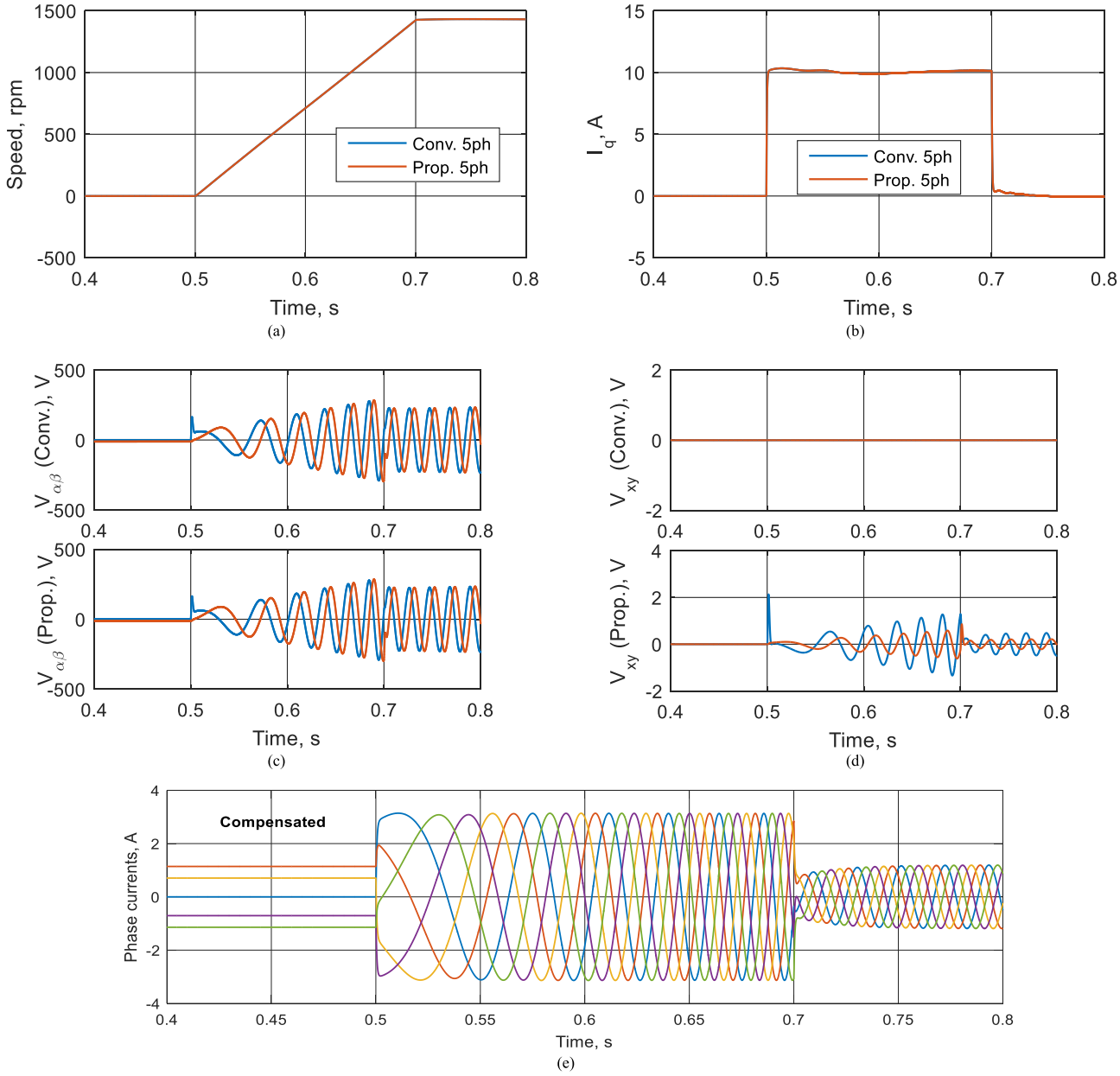

FIGURE 16. Five-phase (18-slot) dynamic response under step quadrature current component and torque control mode with secondary current compensation. (a) Speed. (b) Torque. (c) $V_{\alpha\beta}$ components. (d) V_{xy} components. (e) Phase currents.

stator frame. This case represents the step response of this electromechanical system. Second, the machine mathematical model under IRFOC based on the calculated inductance matrix is built and used to simulate the dynamic response of different winding layouts using MATLAB /SIMULINK.

A. MACHINE START-UP USING FEA

First, the transient module in JMAG FEA software is used to simulate the startup response of the machine while the rated voltage is applied to the stator. This is carried out for the original 3-phase machine and with the same stator equipped with the proposed 5-, 7-, and 11-phase winding layouts. The rated voltages for different n-phase windings are given in section III. All cases assume the same total number of turns to ensure a fair comparison. However, the number of stator slots are adjusted based on the employed winding layout. The speed, as well as the torque responses for all cases, are shown in Fig. 14. Clearly, all stators with a number of phases higher than three have a quicker speed response than the original three-phase case, thanks to the obtained torque gain due to winding factor improvement when multiphase winding layouts are generally engaged [20]. This FE simulation study clearly proves that the proposed winding will correspond to a step dynamic performance even better than the three-phase

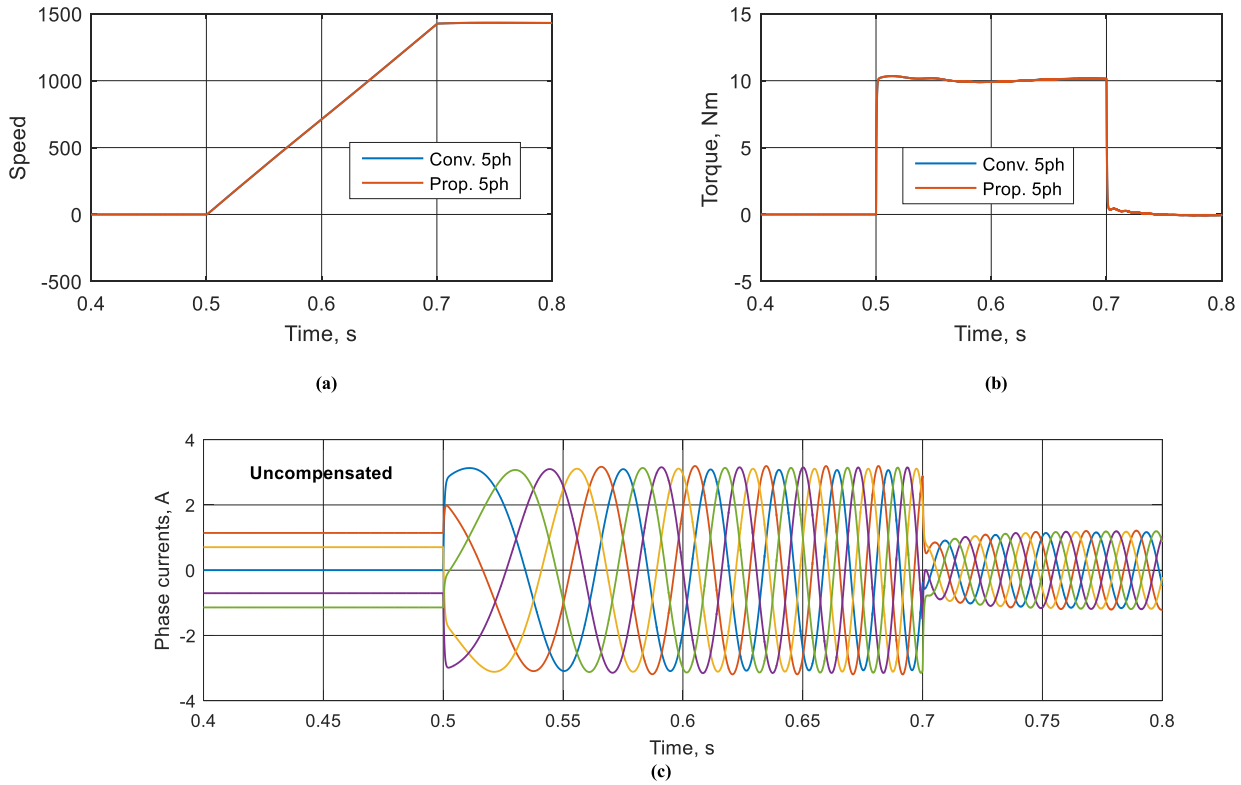

FIGURE 17. Five-phase (18-slot) dynamic response under step quadrature current component and torque control mode without secondary current compensation (V_{xy}1-2 = 0). (a) Speed. (b) Torque. (c) Phase currents.

case, regardless of any possible small stator impedance imbalance. The 24-slot seven-phase stator is slightly better than the 18-slot; the latter experiences a higher stator impedance unbalance yielding to a slightly lower torque producing component.

B. MATHEMATICAL MODELLING AND DYNAMIC SIMULATION

In this subsection, the derived sequence stator leakage inductance matrices in section III are used to build the machine mathematical model given as follows.

The machine sequence voltage equations are given in matrix form as;

$$\left[v^n_{s\alpha\beta}\right] = \left[R^n_s\right]\left[i^n_{s\alpha\beta}\right] + \frac{d}{dt}\left[\lambda^n_{s\alpha\beta}\right] \tag{30}$$

$$[0] = \left[R^n_r\right]\left[i^n_{r\alpha\beta}\right] + \frac{d}{dt}\left[\lambda^n_{r\alpha\beta}\right] + \left[G^n\right]\omega_r\left[\lambda^n_{r\alpha\beta}\right] \tag{31}$$

where the impedance matrices dimension is $n \times n$, while the sequence vector $\left[x^n_{\alpha\beta}\right]$, which may be representing voltage, current, or flux linkage, is defined as $\left[x^n_{\alpha\beta}\right] = \left[\, x_{\alpha 1}\ x_{\beta 1}\ x_{x1}\ x_{y1}\ \ldots\ x_{x(n-2)}\ x_{y(n-2)}\ x_0 \,\right]^t$.

The resistance and conductance matrices are defined as in terms of different subspace parameters as

$$\left[R^n_s\right] = diag\left(\left[\, r_s\ \ldots\ r_s\ r_s \,\right]\right),$$
$$\left[R^n_r\right] = diag\left(\left[\, r_{r1}\ r_{r1}\ r_{r3}\ r_{r3}\ \ldots\ r_{r(n-2)}\ r_{r(n-2)}\ 0 \,\right]\right),$$

r_{rj} is the rotor resistance of subspace j, and

$$\left[G^n\right] = diag\left(\left[\begin{bmatrix} 0 & 1 \\ -1 & 0 \end{bmatrix}\begin{bmatrix} 0 & 3 \\ -3 & 0 \end{bmatrix}\cdots\begin{bmatrix} 0 & n-2 \\ 2-n & 0 \end{bmatrix} 0\right]\right)$$

The flux linkage equations are defined by (32) and (33).

$$\left[\lambda^n_{s\alpha\beta}\right] = \left[L^n_s\right]\left[i^n_{s\alpha\beta}\right] + \left[L^n_m\right]\left[i^n_{r\alpha\beta}\right] \tag{32}$$

$$\left[\lambda^n_{r\alpha\beta}\right] = \left[L^n_r\right]\left[i^n_{r\alpha\beta}\right] + \left[L^n_m\right]\left[i^n_{s\alpha\beta}\right] \tag{33}$$

The inductance matrices are given by

$$\left[L^n_s\right] = \left[L^n_{ls}\right] + \left[L^n_{lm}\right] + \left[L^n_m\right] \tag{34}$$

$$\left[L^n_r\right] = \left[L^n_{lr}\right] + \left[L^n_m\right] \tag{35}$$

where,

$\left[L^n_{ls}\right]$ is the stator self-leakage inductance matrix,
$\left[L^n_{lm}\right]$ is the stator mutual-leakage inductance matrix,
$\left[L^n_{lr}\right]$ is the rotor self-leakage inductance matrix, and
$\left[L^n_m\right]$ is the magnetizing inductance matrix,

The stator self and mutual leakage inductances are found as given by the derivation given in section III. While the rotor leakage and magnetizing inductance matrices are defined as;

$$\left[L^n_{lr}\right] = diag\left(\left[\, l_{r1}\ l_{r1}\ l_{r3}\ l_{r3}\ \ldots\ l_{r(n-2)}\ l_{r(n-2)}\ 0 \,\right]\right),$$

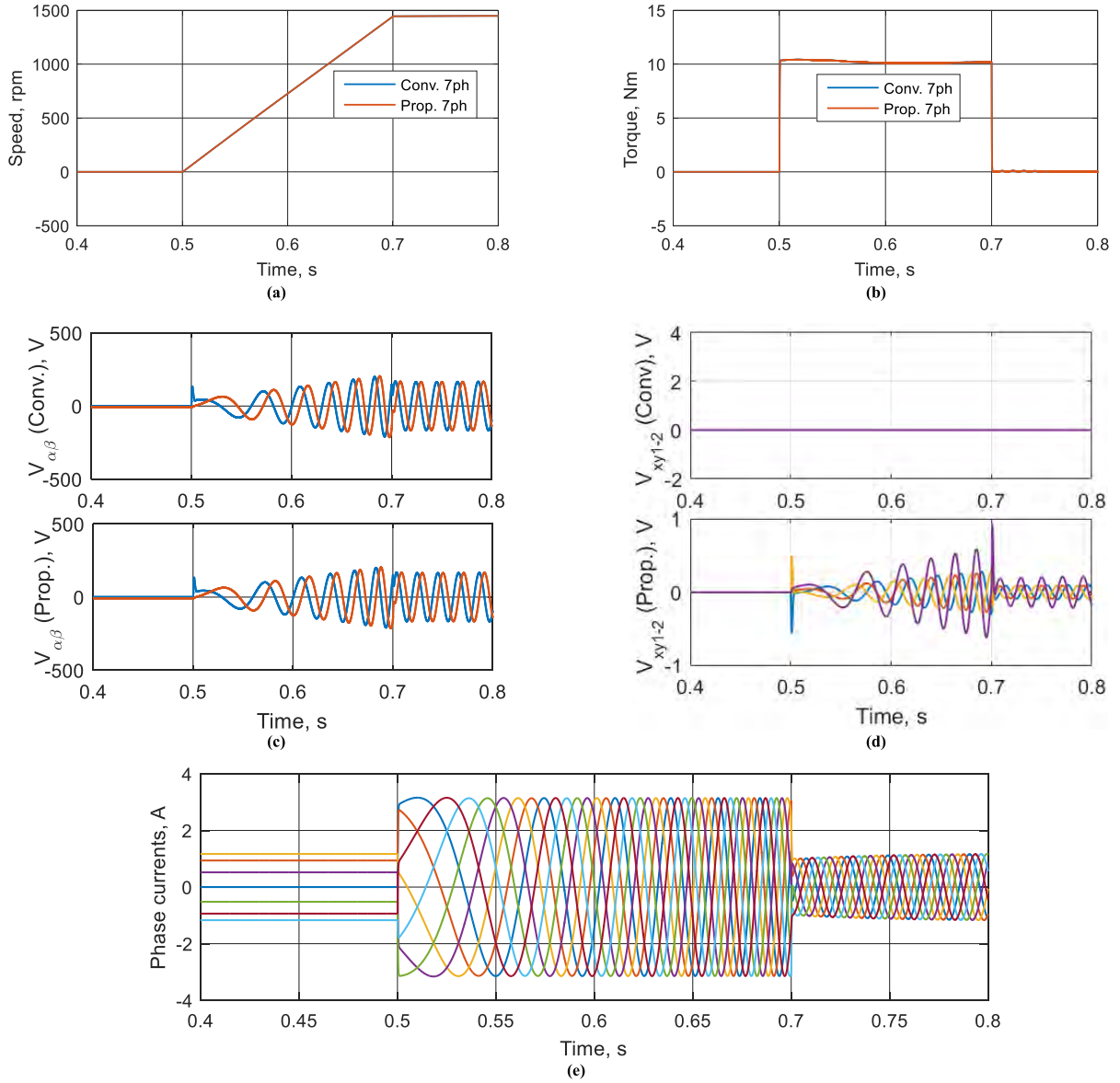

FIGURE 18. Seven-phase machine (24-slot stator). (a) Speed. (b) Torque. (c) $V_{\alpha\beta}$ components. (d) V_{xy} components. (e) Phase currents.

l_{rj} is the rotor leakage inductance of subspace j, and

$$\left[L_m^n\right] = diag\left(\left[\, L_{m1}\ L_{m1}\ L_{m3}\ L_{m3}\ \ldots\ L_{m(n-2)}\ L_{m(n-2)}\ 0\,\right]\right),$$

The average torque, T_e, expression can be calculated from;

$$T_e = \frac{n}{2} p \left[i_{r\alpha\beta}^n\right]^t \left[G^n\right] \left[\lambda_{r\alpha\beta}^n\right] \tag{36}$$

The previous model can be used to simulate the effect of stator leakage inductance mismatch for any phase order n. This is will be done first for the five-phase prototype machine. Then the simulation study is extended to investigate the other phase orders.

In order to obtain the parameters for the five-phase prototype machine, the parameters of different subspaces of the prototype machine are first identified using the technique given in [28]. Based on the estimated machine parameters, different inductance terms are identified to build the required machine model. The main challenge is to separate different stator leakage inductance terms from the lump sum of the stator leakage inductance obtained based on the blocked rotor test. Based on the derivation given in section III.B, the coefficient k_{mtb} given by (14) can be used to separate the leakage inductance terms from the lump sum of the stator leakage inductance obtained based on conventional blocked rotor test.

The machine dynamic response is investigated based on IRFOC for an n-phase machine and given in Fig. 15 [2]. The machine speed and torque responses are obtained while controlling the machine in torque mode under step reference quadrature current component. The reference direct current component is set to 1.2 A (rated magnetizing current component). At 0.5s, the reference quadrature current

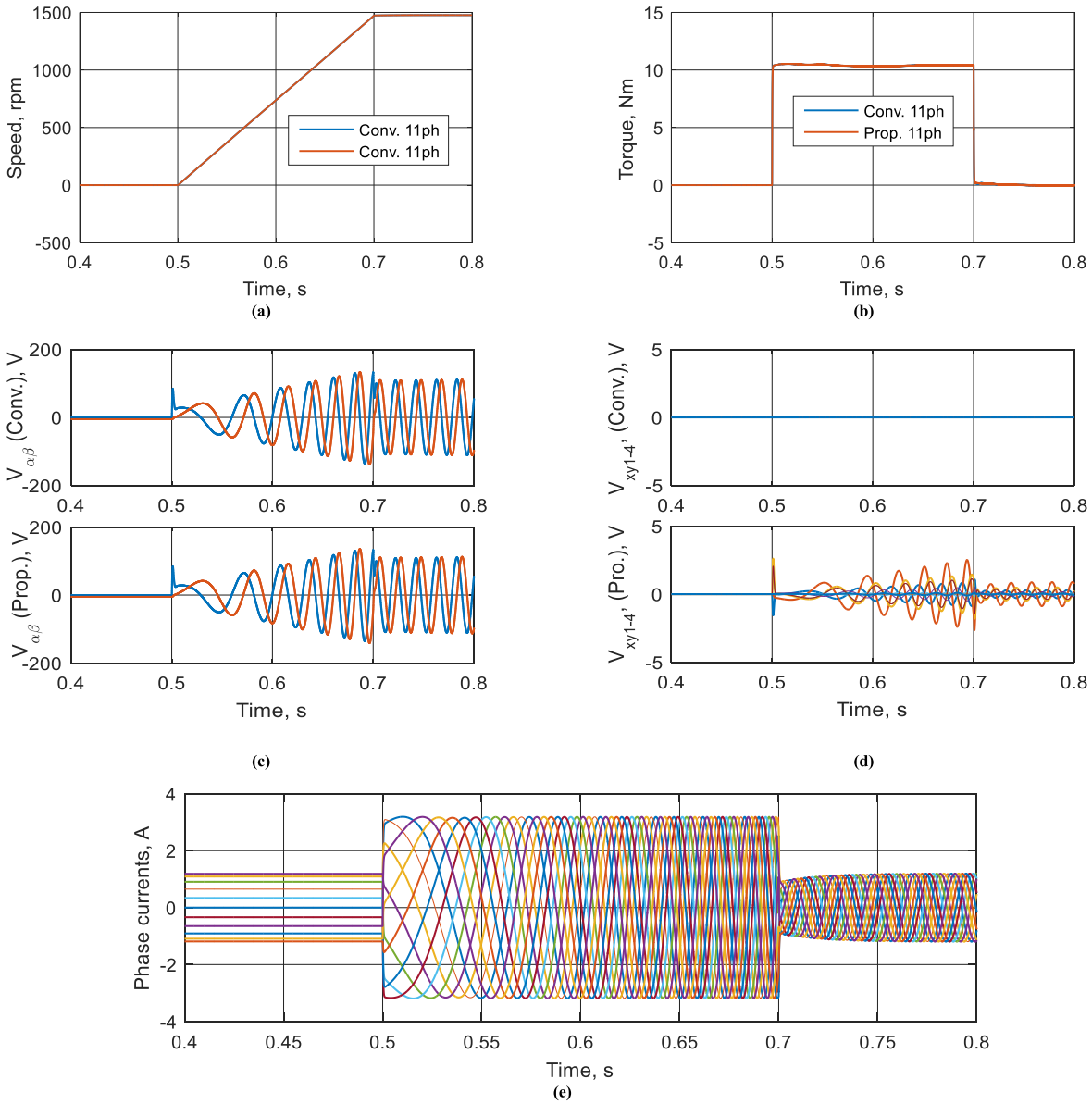

FIGURE 19. Eleven-phase case (24-slot stator). (a) Speed. (b) Torque. (c) $V_{\alpha\beta}$ components. (d) V_{xy} components. (e) Phase currents.

component is step-increased from zero to 2A then brought back to 0 after 0.2s. Two cases are considered, namely with the *xy* current components controlled to zero (compensated case) and with the *xy* voltage components set to zero (uncompensated cases). A pair of PI current controllers are used to regulate each subspace with a total of 4-PI controllers for the five-phase case. All PI gains of the current controllers are selected to be the same for the proposed and the standard five-phase machines.

For the prototype five-phase machine, the simulation results of the conventional and the proposed windings for the compensated and uncompensated cases are shown in Figs. 16 and 17, respectively. Clearly, the proposed and the conventional five-phase windings give identical dynamic responses. Under the compensated case, the *xy* current controllers produce small V_{xy} components to ensure zero *xy* current components and, hence, perfect balanced phase currents are eventually obtained. While, under the uncompensated case, the *xy* current controllers are disabled while the V_{xy} components are simply set to zero. This will give rise to small *xy* current components, which yields a small current imbalance, as clear from Fig 17(c). However, this small unbalance has nothing to do with the machine dynamic response.

The same simulation case has been repeated for the seven- and eleven-phase stators. The conventional and the proposed windings are compared under the same conditions. The controller block diagram given by Fig. 15 is extended to allow for the extra available subspaces. Based on the original prototype five-phase machine, set of parameters have been estimated for the seven- and eleven-phase machines to ensure the same machine power and current ratings, as explained in [23].

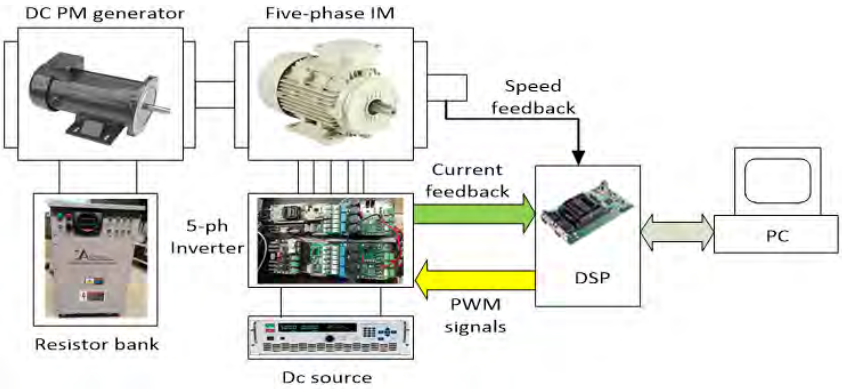

FIGURE 20. Experimental setup block diagram.

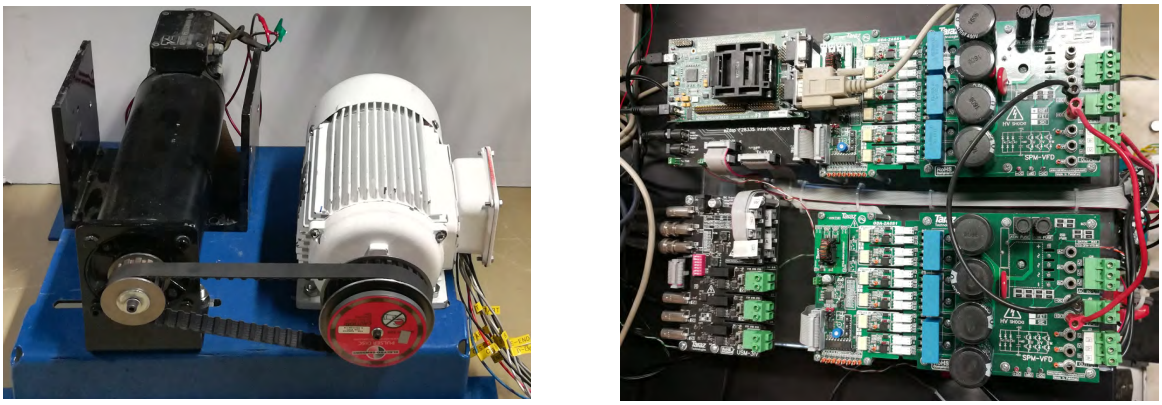

(a) (b)

FIGURE 21. Experimental setup. (a) Five-phase IM. (b) Inverter.

The assumptions made in [23] neglect the small differences in machine inductances due to winding layout and stator design; however, these assumptions may seem appropriate to carry out this comparative study. The considered simulation case studies are given for the compensated case only to avoid repetition. The simulation results are given in Figs. 18 and 19, respectively. Clearly and similar to the five-phase case, the torque and speed curves for the conventional and the proposed winding layouts are quite similar. Since all machines have the same power ratings, the machine accelerating torque and the final steady-state speed will approximately be the same for the same reference *dq* current components. The current controllers produce small *xy* voltage components to compensate for the small impedance mismatch ensuring balanced phase currents under all conditions.

To sum up, the small unbalance in stator leakage inductance between phases will only cause a small current unbalance. This current unbalance can easily be eliminated through current control. Nevertheless, it neither has an effect on the torque production nor on the machine dynamic response.

V. EXPERIMENTAL VALIDATION

In this section, the five-phase prototype machine employed in this study is used to verify the machine model introduced in section VI based on the calculated inductance matrices given in section III. The machine is coupled to a dc generator for mechanical loading. A five-phase inverter controlled using sinusoidal pulse width modulation is used to feed the induction motor. The block diagram of the experimental setup is shown in Fig. 20, while the prototype five-phase induction motor and the power converter are shown in Fig. 21. The machine is controlled using the IRFOC shown in Fig. 15 under speed mode, which is implemented using a Digital Signal Processor (DSP) board eZdspTM based on the Texas Instruments F28335 DSP. The current components of the secondary subspace i_{dq3} are controlled to zero. While the reference direct component is set to 1.2 A. The machine reference speed is firstly set to 500 rpm while accelerated mechanically unloaded. The reference speed is then step-increased to 1000 rpm. The full load torque is then applied by loading the dc generator using a resistive load.

The simulated dynamic response for this case is shown in Fig. 22. While the comparison between the experimental and the simulation results based on the proposed mathematical model is shown in Fig. 23. Clearly, the conventional IRFOC can successfully eliminate the induced secondary current components caused by the small unbalance in the stator impedance of different phases. Besides, this unbalance has nothing to do with the machine dynamic response, which seems quite similar to the response of a conventional

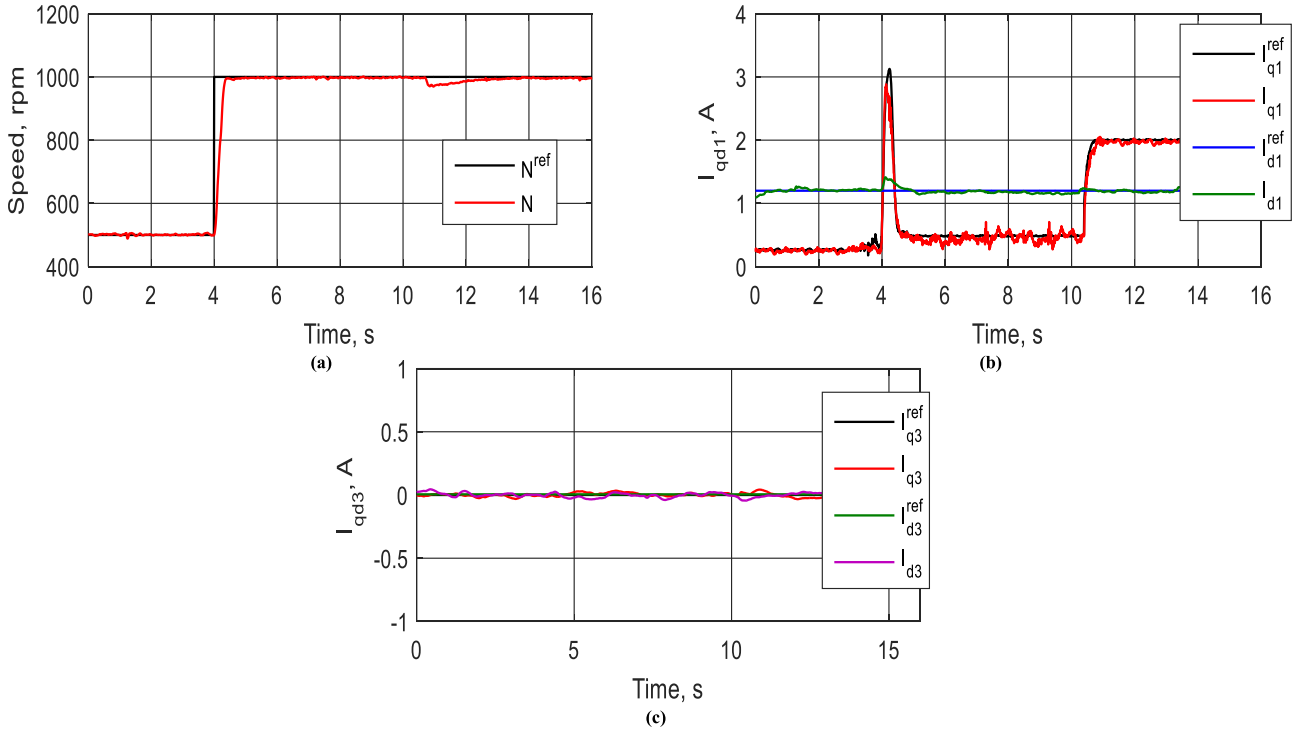

FIGURE 22. Dynamic performance under IRFOC. (a) Speed. (b) dq1 current components. (c) dq3 current components.

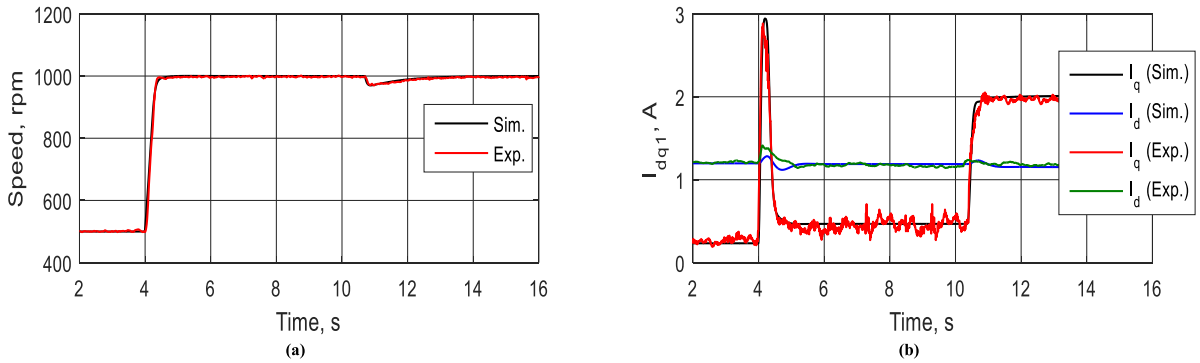

FIGURE 23. Comparison between simulation and experimental results of dynamic performance under IRFOC. (a) Speed. (b) dq1 current components.

symmetrical five-phase machine, as supported by the simulation study given in section IV.

VI. CONCLUSION

This paper investigates the possible slot/pole combinations of standard three-phase stator frames used to construct a multiphase machine of prime-phase order. For a given phase order, some slot/pole combinations have mathematically proven to be optimal in their ability to minimize the stator current unbalance due to the small mismatch in the stator leakage inductance of different phases due to the effect of mutual leakage in a multilayer winding. As a general conclusion, the optimal slot/pole is the one which is close to the slot/pole combination employed for standard n -phase symmetrical winding. It has also been mathematically proven that the small mismatch in stator leakage inductance between phases has nothing to do with the machine dynamic response. Hence, conventional VSD based controllers can successfully be employed. This has been proven by calculating the stator leakage inductance matrices then decomposing them using conventional VSD employed in a symmetrical n -phase winding. The results showed a neglected cross-coupling between different subspaces, especially for optimal slot/pole combinations. This small cross-coupling may, however, yield induced secondary current components due to this impedance mismatch. Nevertheless, these secondary current components can easily be compensated through current control. The mathematical modeling of the proposed winding layouts was also given and verified experimentally using a prototype five-phase machine.

REFERENCES

[1] M. J. Duran, E. Levi, and F. Barrero, "Multiphase electric drives: Introduction," in *Wiley Encyclopedia of Electrical and Electronics Engineering*. New York, NY, USA: Wiley, Nov. 2017.

[2] E. Levi, R. Bojoi, F. Profumo, H. A. Toliyat, and S. Williamson, "Multiphase induction motor drives—A technology status review," *IET Electr. Power Appl.*, vol. 1, no. 4, pp. 489–516, Jul. 2007.
[3] Y. Yu, X. Sun, and W. Zhang, "Modeling and decoupling control for rotor system in magnetic levitation wind turbine," *IEEE Access*, vol. 5, pp. 15516–15528, 2017.
[4] X. Sun, Z. Jin, S. Wang, Z. Yang, K. Li, Y. Fan, and L. Chen, "Performance improvement of torque and suspension force for a novel five-phase BFSPM machine for flywheel energy storage systems," *IEEE Trans. Appl. Supercond.*, vol. 29, no. 2, Mar. 2019, Art. no. 0601505.
[5] X. Sun, K. Diao, G. Lei, L. Chen, Y. Guo, and J. Zhu, "Study on segmented-rotor switched reluctance motors with different rotor pole numbers for BSG system of hybrid electric vehicles," *IEEE Trans. Veh. Technol.*, to be published.
[6] X. Sun, B. Su, S. Wang, Z. Yang, G. Lei, J. Zhu, and Y. Guo, "Performance analysis of suspension force and torque in an IBPMSM with V-shaped PMs for flywheel batteries," *IEEE Trans. Magn.*, vol. 54, no. 11, Nov. 2018, Art. no. 8105504.
[7] X. Sun, C. Hu, J. Zhu, S. Wang, W. Zhou, Z. Yang, G. Lei, K. Li, B. Zhu, and Y. Guo, "MPTC for PMSMs of EVs with multi-motor driven system considering optimal energy allocation," *IEEE Trans. Magn.*, to be published.
[8] X. Sun, Y. Shen, S. Wang, G. Lei, Z. Yang, and S. Han, "Core losses analysis of a novel 16/10 segmented rotor switched reluctance BSG motor for HEVs using nonlinear lumped parameter equivalent circuit model," *IEEE/ASME Trans. Mechatronics*, vol. 32, no. 2, pp. 747–757, Apr. 2018.
[9] Y. Luo and C. Liu, "Model predictive control for a six-phase PMSM motor with a reduced-dimension cost function," *IEEE Trans. Ind. Electron.*, to be published.
[10] M. S. A. Shaikh and R. Maurya, "Realization of 24-sector SVPWM with new switching pattern for six-phase induction motor drive," *IEEE Trans. Power Electron.*, to be published.
[11] S. Dash and S. Kaarthik, "Independent speed control of two parallel connected split-phase IM with a common DC-link and inverter," *IEEE Trans. Power Electron.*, to be published.
[12] E. A. Klingshirn, "High phase order induction motors—Part I-Description and theoretical considerations," *IEEE Trans. Power App. Syst.*, vol. PAS-102, no. 1, pp. 47–53, Jan. 1983.
[13] L. A. Pereira, S. Haffner, G. Nicol, and T. F. Dias, "Multiobjective optimization of five-phase induction machines based on NSGA-II," *IEEE Trans. Ind. Electron.*, vol. 64, no. 12, pp. 9844–9853, Dec. 2017.
[14] A. Tani, M. Mengoni, L. Zarri, G. Serra, and D. Casadei, "Control of multiphase induction motors with an odd number of phases under open-circuit phase faults," *IEEE Trans. Power Electron.*, vol. 27, no. 2, pp. 565–577, Feb. 2012.
[15] M. Mengoni, L. Zarri, A. Tani, L. Parsa, G. Serra, and D. Casadei, "High-torque-density control of multiphase induction motor drives operating over a wide speed range," *IEEE Trans. Ind. Electron.*, vol. 62, no. 2, pp. 814–825, Feb. 2015.
[16] A. Abdel-Khalik, M. I. Masoud, S. M. Gadoue, and B. W. Williams, "Optimum flux distribution with harmonic injection for a multiphase induction machine using genetic algorithms," *IEEE Trans. Energy Convers.*, vol. 26, no. 2, pp. 501–512, Jun. 2011.
[17] K. Wang, Z. Y. Gu, C. Liu, and Z. Q. Zhu, "Design and analysis of a five-phase SPM machine considering third harmonic current injection," *IEEE Trans. Energy Convers.*, vol. 33, no. 3, pp. 1108–1117, Sep. 2018.
[18] A. S. Abdel-Khalik, S. Ahmed, and A. M. Massoud, "Steady-state mathematical modeling of a five-phase induction machine with a combined star/pentagon stator winding connection," *IEEE Trans. Ind. Electron.*, vol. 63, no. 3, pp. 1331–1343, Mar. 2016.
[19] H. Qiu-Liang, C. Yong, and X. Li, "Fault-tolerant control strategy for five-phase PMSM with third-harmonic current injection," *IEEE Access*, vol. 6, pp. 58501–58509, 2018.
[20] A. S. Abdel-Khalik, A. M. Massoud, and S. Ahmed, "Application of standard three-phase stator frames in prime phase order multiphase machine construction," *IEEE Trans. Ind. Electron.*, vol. 66, no. 4, Apr. 2019, pp. 2506–2517.
[21] N. Bianchi and M. D. Pre, "Use of the star of slots in designing fractional-slot single-layer synchronous motors," *IEE Proc.-Electr. Power Appl.*, vol. 153, no. 3, pp. 459–466, May 2006.
[22] P. B. Reddy, K.-K. Huh, and A. M. El-Refaie, "Generalized approach of stator shifting in interior permanent-magnet machines equipped with fractional-slot concentrated windings," *IEEE Trans. Ind. Electron.*, vol. 61, no. 9, pp. 5035–5046, Sep. 2014.
[23] A. Abdel-Khalik, M. Masoud, S. Ahmed, and A. Massoud, "Effect of current harmonic injection on constant rotor volume multiphase induction machine stators: A comparative study," *IEEE Trans. Ind. Appl.*, vol. 48, no. 6, pp. 2002–2013, Nov./Dec. 2012.
[24] A. Tessarolo and D. Giulivo, "Analytical methods for the accurate computation of stator leakage inductances in multi-phase synchronous machines," in *Proc. SPEEDAM*, Pisa, Italy, Jun. 2010, pp. 845–852.
[25] D. Hadiouche, H. Razik, and A. Rezzoug, "On the modeling and design of dual-stator windings to minimize circulating harmonic currents for VSI fed AC machines," *IEEE Trans. Ind. Appl.*, vol. 40, no. 2, pp. 506–515, Mar. 2004.
[26] T. A. Lipo, "A d-q model for six-phase induction machine," in *Proc. Int. Conf. Electr. Mach. (ICEM)*, Athens, Greece, Sep. 1980, pp. 860–867.
[27] Z. Shi, X. Sun, Y. Cai, Z. Yang, G. Lei, Y. Guo, and J. Zhu, "Torque analysis and dynamic performance improvement of A PMSM for EVs by skew angle optimization," *IEEE Trans. Appl. Supercond.*, vol. 29, no. 2, Mar. 2019, Art. no. 0600305.
[28] A. S. Abdel-Khalik, M. I. Daoud, S. Ahmed, A. A. Elserougi, and A. M. Massoud, "Parameter identification of five-phase induction machines with single layer windings," *IEEE Trans. Ind. Electron.*, vol. 61, no. 10, pp. 5139–5154, Oct. 2014.

AYMAN S. ABDEL-KHALIK (SM'12) received the B.Sc. and M.Sc. degrees in electrical engineering from Alexandria University, Alexandria, Egypt, in 2001 and 2004, respectively, and the Ph.D. degree in electrical engineering from Alexandria University and Strathclyde University, Glasgow, U.K., in 2009, under a dual channel program. He is currently an Associate Professor with the Electrical Engineering Department, Faculty of Engineering, Alexandria University, Alexandria, Egypt. He serves as an Associate Editor of *IET Electric Power Applications Journal* and the Executive Editor of *Alexandria Engineering Journal*. His current research interests include electrical machine design and modeling, electric drives, energy conversion, and renewable energy.

AHMED MASSOUD (SM'11) received the B.Sc. (first class honors) and M.Sc. degrees in electrical engineering from Alexandria University, Egypt, in 1997 and 2000, respectively, and the Ph.D. degree in electrical engineering from Heriot-Watt University, Edinburgh, U.K., in 2004. He is currently a Professor at the Department of Electrical Engineering, College of Engineering, Qatar University. His research interests include power electronics, energy conversion, renewable energy, and power quality. He holds five U.S. patents. He published more than 100 journal papers in the fields of power electronics, energy conversion, and power quality.

SHEHAB AHMED (SM'12) received the B.Sc. degree in electrical engineering from Alexandria University, Alexandria, Egypt, in 1999, and the M.Sc. and Ph.D. degrees from the Department of Electrical and Computer Engineering, Texas A&M University, College Station, TX, USA, in 2000 and 2007, respectively. He was with Schlumberger Technology Corporation, Houston, TX, USA, from 2001 to 2007, developing downhole mechatronic systems for oilfield service products. He was with Texas A&M University at Qatar, from 2007 to 2018 (currently on leave). He is currently a Professor of electrical engineering with the CEMSE Division at King Abdullah University of Science and Technology, Saudi Arabia. His research interests include mechatronics, solid-state power conversion, electric machines, and drives.